Numerical Methods for the QCD Overlap Operator IV: Hybrid Monte Carlo

N. Cundy [a], S. Krieg[b, d], G. Arnold [d], A. Frommer [c],
Th. Lippert[b, d] and K. Schilling [b]

[a]*Department of Physics, University of Regensburg, Universitätstraße 31, 93040 Regensburg, Germany.*

[b]*Fachbereich C, Fachgruppe Physik, University of Wuppertal, Gaussstraße 20, 42119 Wuppertal, Germany.*

[c]*Fachbereich C, Fachgruppe Mathematik, University of Wuppertal,Gaussstraße 20 42119 Wuppertal, Germany.*

[d]*Jülich Supercomputing Center, Jülich Research Center, 52425 Jülich, Germany.*

Abstract

The computational costs of calculating the matrix sign function of the overlap operator together with fundamental numerical problems related to the discontinuity of the sign function in the kernel eigenvalues are the major obstacles towards simulations with dynamical overlap fermions using the Hybrid Monte Carlo algorithm. In a previous paper of the present series we introduced optimal numerical approximation of the sign function and have developed highly advanced preconditioning and relaxation techniques which speed up the the inversion of the overlap operator by nearly an order of magnitude.

In this fourth paper of the series we construct an HMC algorithm for overlap fermions. We approximate the matrix sign function using the Zolotarev rational approximation, treating the smallest eigenvalues of the Wilson operator exactly within the fermionic force. Based on this we derive the fermionic force for the overlap operator. We explicitly solve the problem of the Dirac delta-function terms arising through zero crossings of eigenvalues of the Wilson operator. The main advantage of this scheme is that its energy violations scale better than $O(\Delta\tau^2)$ and thus are comparable with the violations of the standard leapfrog algorithm over the course of a trajectory. We explicitly prove that our algorithm satisfies reversibility and area conservation. We present test results from our algorithm on 4^4, 6^4, and 8^4 lattices.

13 August 2018

1 Introduction

For more than two decades lattice QCD simulations with light dynamical quarks remained intractable as the chiral symmetry of the underlying QCD Lagrangian, which holds in the case of zero mass quarks, could not be embedded properly into flavour conserving fermion lattice discretization schemes. A standard workaround takes recourse to fairly heavy quarks instead and extrapolates the results over a wide range of quark masses to the very light quark mass regime. Unfortunately, simulating far beyond the realm of chiral perturbation theory such extrapolations carry systematic errors. These errors have to be avoided in order to achieve a high precision of phenomenological observables. [1]

During the 90's the first chiral lattice Dirac operators were written down. While studying domain wall fermions [2], an early attempt to formulate chiral fermions on the lattice, Neuberger and Narayanan realised that the Nielsen-Ninomiya theorem [3] can be circumvented by placing an infinite number of fermions on the lattice. This insight led them to the overlap lattice Dirac operator [4,5]. Afterwards, Hasenfratz, while working with classically perfect fermions, realised that the small mass bottleneck could be overcome by using a discretization scheme that obeys a lattice variant of chiral symmetry [6], as expressed by the Ginsparg-Wilson relation for the quark propagator [7], which in turn implies a novel version of chiral symmetry on the lattice [8]. Neuberger showed that the overlap operator obeys the Ginsparg-Wilson relation. Theoretically, such a scheme induces a dramatic reduction in fluctuations in the smallest Dirac operator eigenvalue compared to naive Wilson fermions in the vicinity of zero quark mass. However, there is a numerical obstacle: the implementation of the overlap operator requires the very frequent solution of linear systems involving the inverse matrix square root or, equivalently, the matrix sign function (of the Hermitian Wilson-Dirac operator Q).

The problem of approximating the application of $\text{sign}(Q)$ on a vector has been discussed in a number of papers, using polynomial approximations [9,10,11,12,13], Lanczos based methods [14,15,16,17] and multi-shift CG combined with a partial fraction expansion [18,19,20,21]. The Zolotarev partial fraction approximation (ZPFE), first applied to lattice QCD in [22] – the first paper in the present series – was shown to be the optimal approximation to the matrix sign function. ZPFE has led to an improvement of over a factor of 3 compared to the Chebyshev polynomial approach [11]. This technique to compute the sign function has meanwhile been established as the method of choice [23,24,25].

---

[1] Simulations with staggered fermions are less prone to fluctuations. However, it is yet unclear if staggered fermions have the correct continuum limit in case of their one-flavour approximation by the fourth root trick [1].

Moreover, it is the natural starting point for both the treatment of dynamical overlap fermions [26] and optimised domain wall fermions [27,28,29]. [2]

Until recently, simulations with overlap fermions were restricted to the quenched model where fermion loops are neglected [34,35,36,37], or hybrid calculations using staggered or Wilson sea quarks, because of two reasons: (i) the sheer costs of the evaluation of sign functions of matrices with extremely high dimensions and (ii) the lack of exact algorithms including dynamical overlap fermions.

In this paper, we construct a Hybrid Monte Carlo algorithm [38] for QCD with overlap fermions. [3] Mostly, we just need to adapt the algorithm as existing for example for Wilson fermions to the overlap operator. However, the discontinuity in the matrix sign function used in the overlap construction causes additional complications: as soon as one of the eigenvalues of Q crosses zero, the change in the sign of the eigenvalue leads to a discontinuity in the fermionic part of the action, which introduces the occurrence of a Dirac delta function in the HMC fermionic force, as first discussed in [26,43]. This effect is predominantly seen in strong coupling: eigenvalue crossings are rare in the weak coupling limit [45].

The major part of this paper will deal with the proper integration of this singular force. Important new contributions in this paper are: (1) We calculate the energy violation at the crossing exactly; (2) We explicitly treat the implementation of the eigenvalue projection technique in the HMC algorithm; (3) Most importantly, we introduce a momentum update when there is an eigenvalue crossing with improved energy conservation properties, with the leading errors being of order $O(\Delta\tau^2)$. This is based on our generalized scheme to construct higher-order exact treatment of the eigenvalue crossing. We are going to demonstrate that this feature, along with the dependency of the small eigenvalue density leads to an HMC algorithm with computational complexity of $O(V^{5/4})$. (4) We discuss what happens when two eigenvalues cross within the same molecular dynamics step. [4]

The main practical difficulty in running dynamical overlap simulations is the cost in computer time. Overlap fermions are at least $O(100)$ times more expen-

---

[2] An alternative scheme is to use a 5-dimensional representation of the overlap operator – see references [30,31,32]. An HMC algorithm using a polynomial approximation to the sign function was tested in [33], and found to be inferior to the ZPFE.

[3] Earlier work done concerning dynamical overlap fermions in the Schwinger model can be found in [39,40,41,42]. More recently, some exploratory studies in full QCD [26,43,44] have been presented.

[4] In a forthcoming paper we will present an advanced scheme for the treatment of two small eigenvalues.

sive to compute than Wilson fermions. In other papers of this series [46,47,48], we discussed how the inversion of the overlap operator, a very time consuming part of the HMC algorithm, can be accelerated. Here we will make use of all these methods. We estimate the time required with our current algorithms for a full HMC simulation on moderate lattices at realistic masses. Early results were outlined in [49].

Section 2.1 gives a brief introduction to the Hybrid Monte Carlo method for generating dynamical configurations. Sections 2.2 to 4 outline our method for adapting HMC to the overlap operator. Section 5 gives first numerical results, demonstrating that the algorithm works in practice. After a brief conclusion, we include two appendices, proving that the proposed algorithm satisfies detailed balance and describe the additional implications of a combined transmission/reflection update within a normal leapfrog integration. Furthermore we describe the correction update when two eigenvalues cross zero during the same time step.

2 Hybrid Monte Carlo

2.1 HMC for Wilson fermions

In order to make the paper self-contained, we give a short review of the HMC algorithm for the case of Wilson fermions [38].

The standard Wilson Dirac operator on the lattice, with a mass $-m_0$, is

$$
\begin{aligned}
M_{xy} =& 1_{xy} - \kappa \sum_\mu \Big[\left(1 - \gamma_\mu\right) U_\mu(x)\delta_{x+e_\mu,y} \\
&+ \left(1 + \gamma_\mu\right) U^\dagger{}_\mu(x - e_\mu)\delta_{x-e_\mu,y} \Big], \\
\kappa =& \frac{1}{8 - 2m_0}.
\end{aligned}
\tag{1}
$$

The Wilson operator is γ_5-Hermitian, implying that one can construct a Hermitian Wilson operator

$$
Q = \gamma_5 M.
\tag{2}
$$

The HMC method updates the gauge field in two steps: (1) a molecular dynamics evolution of the gauge field and (2) a Metropolis step which renders the algorithm exact. In the molecular dynamics step, a momentum Π is introduced, which is conjugate to the gauge fields U. Using a fictitious computer

time, τ, the momentum field is defined such that

$$dU/d\tau = \dot{U} = i\Pi U. \tag{3}$$

Since $U \in \mathrm{SU}(N_C)$, Π must be a Hermitian traceless matrix. Following the classical equations of motion of this system will allow to generate the correct ensemble. Using the Wilson gauge action, the total energy of this system is

$$E(\tau) = \beta \sum_x \left[1 - \frac{1}{2N_C} Tr\left(U(x)_{\mu\nu} + U(x)_{\mu\nu}^\dagger \right) \right] + X_W^\dagger \Phi + \frac{1}{2} \sum \mathrm{Tr}\Pi^2, \tag{4}$$

$$X_W = Q^{-2}\Phi. \tag{5}$$

$U(x)_{\mu\nu}$ is called the plaquette, Φ is a Gaussian random spinor field, and N_C is the number of colours (for QCD $N_C = 3$). The second equation of motion can be inferred from the condition

$$\dot{E} = 0$$
$$= \sum_{x,\mu} \mathrm{Tr} \left[\frac{1}{2} \frac{d}{d\tau} (\Pi_\mu(x)^2) - i \left(\frac{\beta}{6} \Pi_\mu(x) U_\mu(x) V_\mu(x) + \Pi_\mu(x) F_\mu(x) - h.c. \right) \right]. \tag{6}$$

This leads to

$$\dot{\Pi}_\mu(x) = i \left[\left(\frac{\beta}{6} U_\mu(x) V_\mu(x) + F_\mu(x) - h.c. \right) \right]_{\mathrm{Traceless}}. \tag{7}$$

Here $V_\mu(x)$ is the staple, the sum over all the remaining parts of those plaquettes which contain the specific gauge link $U_\mu(x)$. $F_\mu(x)$ is the fermionic force, which can be found by differentiating $X_W^\dagger \Phi$ with respect to $U_\mu(x)$. For Wilson fermions, the fermionic force is given by

$$F_\mu(x) = \kappa \left[\left(MX_W \right)_{x+e_\mu} X_W^\dagger(x)(1 + \gamma_\mu) + X_W(x + e_\mu) \left(MX_W \right)^\dagger(x)(1 - \gamma_\mu) \right]. \tag{8}$$

These classical equations of motion have to be solved numerically. An important requirement for the Markov process is to maintain *detailed balance*, in order to guarantee the generation of the correct canonical distribution. To maintain detailed balance, each molecular dynamics update from computer time τ to computer time $\tau + \Delta\tau$ needs to be both area conserving, *i.e.* the Jacobian for the update is 1, and reversible.[5] The leapfrog algorithm fulfils both these requirements, and, over an entire trajectory, conserves energy up to

---

[5] Starting with a configuration $\{U(0), \Pi(0)\}$, we perform a molecular dynamics step to reach a configuration $\{U(\Delta\tau), \Pi(\Delta\tau)\}$. If the update is reversible, carrying out the molecular dynamics step backwards, with $\Delta\tau \to -\Delta\tau$ and $\Pi \to -\Pi$, will return to the original configuration.

(1) $\Pi(\tau + \Delta\tau/2) = \Pi(\tau) + \Delta\tau \dot{\Pi}(\tau)/2.$
(2) $U(\tau + \Delta\tau/2) = e^{i(\Delta\tau/2)\Pi(\tau+\Delta\tau/2)}U(\tau).$
(3) $U(\tau + \Delta\tau) = e^{i(\Delta\tau/2)\Pi(\tau+\Delta\tau/2)}U(\tau + \Delta\tau/2).$
(4) $\Pi(\tau + \Delta\tau) = \Pi(\tau + \Delta\tau/2) + \Delta\tau \dot{\Pi}(\tau + \Delta\tau)/2.$

Algorithm 1. The standard leapfrog update.

order $\Delta\tau^2$.[6] For later convenience, we will write it in terms of a four-step procedure updating the momentum fields and gauge fields in turn (see algorithm 1). The HMC update consists of n_{md} molecular dynamics steps followed by a Metropolis step, which corrects for the small violations in energy conservation due to the numerical integration. At the end of the trajectory, the configuration is either accepted or rejected, with the probability of acceptance being $P_{\mathrm{acc}} = \min(1, \exp(E - E'))$. Here E is the initial energy at the start of the trajectory, and E' the final energy. To generate a sufficiently large number of new configurations, a high rate of acceptance is required. Thus, the molecular dynamics procedure has to conserve energy as well as possible. Any sizable violation of energy conservation will lower the acceptance rate, and thus the efficiency of the algorithm.

2.2 Naive HMC with overlap fermions

The overlap operator is given by [18]:

$$D = (1 + \mu) + \gamma_5(1 - \mu)\,\mathrm{sign}(Q), \tag{9}$$

where μ is a mass term. The bare fermion mass is

$$m_b = 2\mu m_0/(1 - \mu), \tag{10}$$

where m_0 is the quark mass of the Wilson operator $D_W = \gamma_5 Q$.
The Hermitian overlap operator reads

$$H = \gamma_5 D. \tag{11}$$

Thus, the pseudo-fermion action is given by $S_{pf} = \phi^\dagger H^{-2}\phi$.

---

[6] There are superior integrators to the simple leapfrog, such as the Omelyan integrator [50,51], and the Sexton-Weingarten Integrator [52], but the methods described here can easily be adapted to these integrators; indeed we are using the Omelyan integrator in our current production algorithm.

2.2.1 Eigenvalues outside Zolotarev range.

We approximate the matrix sign function using a rational approximation. It is advantageous while calculating the sign function to treat the smallest eigenvalues of Q explicitly in a spectral representation. If we project out the lowest n_e eigenvectors of Q, then the rational fraction expansion, which is used to approximate the sign function for the eigenvalues of Q^2 within the fixed range $[\alpha^2, \beta^2]$, is modified to

$$\text{sign}(Q) = aQ \sum_k A^k \omega_k(\alpha, \beta) \left(1 - \sum_{l=1}^{n_e} |\psi^l\rangle \langle \psi^l| \right) + \sum_{l=1}^{n_e} |\psi^l\rangle \langle \psi^l| \epsilon(\lambda_l), \quad (12)$$

$$A^k = \frac{1}{a^2 Q^2 + \zeta_k(\alpha, \beta)}. \quad (13)$$

Here $a = 1/\alpha$, $|\psi^l\rangle$ are the eigenvectors of Q with eigenvalue λ_l, and $\epsilon(\lambda)$ denotes the sign function. We shall assume that ω and ζ, the coefficients of the rational fraction, are known (here we used the Zolotarev coefficients [53,54]). During the course of the Hybrid Monte Carlo, we keep the coefficients α and β fixed to maintain the acceptance rate, which requires the projection of all eigenvectors of Q with eigenvalues $|\lambda| < \alpha$.

2.2.2 Eigenvalues inside Zolotarev range.

Of course, one is free to project out eigenvectors within the Zolotarev range as well, either exactly, as in (12), or from the rational approximation itself:

$$\sum_k \frac{\omega_k}{a^2 Q^2 + \zeta_k} = \sum_k \frac{\omega_k}{a^2 Q^2 + \zeta_k} \left(1 - \sum_{l=n_e+1}^{n_p} |\psi^l\rangle \langle \psi^l| \right) +$$
$$\sum_{l=n_e+1}^{n_p} |\psi^l\rangle \langle \psi^l| \sum_k \frac{\omega_k}{a^2 \lambda_l^2 + \zeta_k}. \quad (14)$$

This accelerates the calculation of the multi-mass solver. Our preferred method that allows to simply fulfil the requirements for detailed balance, is to project out a fixed number, n_p, of eigenvectors, treating the n_e eigenvectors below α explicitly according to (12), and using (14) for any eigenvectors that lie within the range of the rational fraction approximation.

2.2.3 Differentiating Eigenvectors.

In order to calculate the fermionic force one needs to differentiate the sign function with respect to fictitious time τ, which means that one must differentiate both the rational fraction and the small eigenvalues and eigenvectors.

To differentiate the eigenvalues, we start with the eigenvalue equation

$$Q|\psi^l\rangle = \lambda_l|\psi^l\rangle. \tag{15}$$

We now perform an infinitesimal change in the matrix Q, $Q \to Q + \delta Q$. The new eigenvalue equation reads

$$(Q + \delta Q)\left(|\psi^l\rangle + |\delta\rangle\right) = (\lambda_l + \delta\lambda)\left(|\psi^l\rangle + |\delta\rangle\right). \tag{16}$$

Since we are free to define $|\delta\rangle$ so that $\langle\psi^l|\delta\rangle = 0$, we immediately have:

$$\dot{\lambda}_l = \langle\psi^l|\dot{Q}|\psi^l\rangle \tag{17}$$

$$\frac{d}{d\tau}|\psi^l\rangle = -P_l\dot{Q}|\psi^l\rangle \tag{18}$$

$$P_l = (1 - |\psi^l\rangle\langle\psi^l|)(Q - \lambda_l)^{-1}(1 - |\psi^l\rangle\langle\psi^l|). \tag{19}$$

We have added a second eigenvector projector to (19) so that both $\langle\phi|P_l$ and $P_l|\phi\rangle$ can be calculated numerically.[7] We note that this expansion is only valid if the separation between the eigenvalues is sufficiently large (see appendix B). We will treat the case when the two eigenvalues are near degenerate in a forthcoming paper [55,56].

We use a CG multi-mass solver to perform the inversion of $Q - \lambda$ which is required in (18). We exploit the normal-equation trick:

$$\frac{1}{Q - \lambda_i}(1 - |\psi_i\rangle\langle\psi_i|) = (Q + \lambda_i)\frac{1}{Q^2 - \lambda_i^2}(1 - \sum_{j=1}^{n_p}|\psi_j\rangle\langle\psi_j|) +$$
$$\sum_{j=1;j\neq i}^{n_p}|\psi_j\rangle\langle\psi_j|\frac{\lambda_j + \lambda_i}{\lambda_j^2 - \lambda_i^2},$$

to convert the inversion of $Q - \lambda_i$ required in the calculation of $\frac{d}{d\tau}|\psi^l\rangle$ as given in (18) into a positive definite form—we are working in a subspace orthonormal to all the eigenvectors with eigenvalues lower than λ_i. We can now use a CG multi-mass solver to evaluate the inversion. With a sufficiently large number of kernel eigenvalues projected out of the Zolotarev approximation, this procedure proved to be faster and more stable than using a Minimal Residual inversion or a Chebyshev approximation of the inverse [57] for each eigenvector. The multi-mass inversion converges well, as long as we project into the subspace frequently enough during the inversion, and n_p is sufficiently larger than n_e to ensure that the condition number of the multi-mass inversion remains under control. Tuning α is therefore a balancing act between different

---

[7] These equations are just used to calculate the fermionic force. We cannot use the updates to provide a time evolution of the eigenvectors, for reasons of reversibility, computer time and accuracy.

parts of the algorithm: a large α will correspond to a slower multi-mass inversion for the eigenvector differentiation (because we will be increasing the condition number for the inversion), but a faster inversion for the sign function (since the Zolotarev weights generally increase as the condition number decreases).

The eigenvectors have to be determined whenever we calculate the fermionic force. We used the Arnoldi PARPACK package with Chebyshev acceleration [58,59] to calculate the lowest eigenvalues, and a CG minimisation of the Ritz functional [60] to ensure that no small eigenvectors were missed by the Arnoldi, and that all the eigenvalues were calculated to the required accuracy. This method proved to be considerably faster than using entirely a CG minimisation, even though we can use the old eigenvectors as a starting point for the new calculation when using the CG algorithm.

We are now in a position to calculate the fermionic force in the usual manner (sums over k, l and repeated spatial indices μ and x will be assumed from this point onwards):

$$\dot{U}_\mu(x)F_\mu(x) + F_\mu^\dagger(x)\dot{U}_\mu^\dagger(x) = -(1-\mu^2)\langle X| \left(\gamma_5 \frac{d}{d\tau}\mathrm{sign}\,Q + \frac{d}{d\tau}\mathrm{sign}\,Q\gamma_5\right)|X\rangle,$$
(20)

$$X = H^{-2}\phi.$$
(21)

The differential of the sign function is:

$$\left(\frac{d}{d\tau}\mathrm{sign}\,Q\right)_{nm} = \dot{U}_\mu(x)\left[\tilde{F}^R_{\mu,nm}(x) + \tilde{F}^P_{\mu,nm}(x) + \tilde{F}^S_{\mu,nm}(x) + \tilde{F}^D_{\mu,nm}(x)\right] + h.c.,$$
(22)

where $\tilde{F}^R$ is the term generated by differentiating the rational approximation, $\tilde{F}^P$ is the term generated by differentiating the eigenvector projector $1 - |\psi^l\rangle\langle\psi^l|$, while $\tilde{F}^S$ and $\tilde{F}^D$ come from the differential of $\epsilon(\lambda)$ in (12). These four terms are:

$$\tilde{F}^R_{\mu,nm}(x) = \kappa a \omega_\eta A^k_{na}\left[a^2 Q_{ax}\gamma_5(1-\gamma_\mu)\delta_{x+e_\mu,c}Q_{cd}\right.$$
$$\left. - \zeta_k\gamma_5(1-\gamma_\mu)\delta_{a,x}\delta_{x+e_\mu,d}\right]A^k_{de}\left(1 - |\psi^l\rangle\langle\psi^l|\right)_{em},$$
$$\tilde{F}^P_{\mu,nm}(x) = -\kappa Q A^k_{na}P_{l,ax}\gamma_5(1-\gamma_\mu)\delta_{x-e_\mu,c}\left(|\psi^l\rangle\langle\psi^l|\right)_{cm}$$
$$-\kappa Q A^k_{na}\left(|\psi^l\rangle\langle\psi^l|\right)_{ax}\gamma_5(1-\gamma_\mu)\delta_{x,c+e_\mu}P_{l,cm},$$
$$\tilde{F}^S_{\mu,nm}(x) = \kappa P_{l,nx}\gamma_5\epsilon(\lambda_l)(1-\gamma_\mu)\delta_{x,c+e_\mu}\left(|\psi^l\rangle\langle\psi^l|\right)_{cm}$$
$$+\kappa\left(|\psi^l\rangle\langle\psi^l|\right)_{nx}\gamma_5(1-\gamma_\mu)\delta_{x,c+e_\mu}\epsilon(\lambda_l)P_{l,cm},$$
$$\tilde{F}^D_{\mu,nm}(x) = -\left(|\psi^l\rangle\langle\psi^l|\right)_{nm}\frac{d\epsilon(\lambda_l)}{d\lambda_l}\langle\psi^l|_x\gamma_5(1-\gamma_\mu)\delta_{x,c+e_\mu}|\psi^l\rangle_c. \quad (23)$$

For later convenience, we define F^G as the gauge field force, and F^C as the continuous part of the fermionic force, i.e.,

$$F_\mu^G(x) = \langle X|i\frac{\beta}{6}U_\mu(x)V_\mu(x)|X\rangle + h.c. \,, \tag{24}$$

$$F_\mu^C(x) = -(1-\mu^2)iU_\mu(x)\langle X|\left\{\gamma_5, \tilde{F}_\mu^R(x) + \tilde{F}_\mu^P(x) + \tilde{F}_\mu^S(x)\right\}|X\rangle + h.c. \,. \tag{25}$$

In order to calculate the fermionic force, we need to invert the overlap operator twice, perform two multi-mass inversions of the Zolotarev rational function, and, as remarked before, calculate four multi-mass inversions of the Wilson operator to obtain the force from the small eigenvalue projection. This formula can be inserted into a standard HMC routine for Wilson or staggered fermions. However, the last term in (23) contains a Dirac delta function (the derivative of the sign function) that will ruin the performance of standard integrators. Whenever an eigenvalue of the Wilson operator crosses zero on a HMC trajectory, special attention has to be paid to this last term. We note in passing that eigenvalue crossings of the Wilson operator are associated with a change in the topological index $Q_f = -\frac{1}{2}\text{Tr}(\text{sign}\,Q)$.

3 Eigenvalue Crossings

3.1 Possible strategies

There are several possibilities which can be taken to overcome the problem of the eigenvalue crossing:

(1) Ignore the problem in the hope that it will vanish with increasing values of β. In this spirit, one would use chiral projection [39,61,62] to allow for sampling across different topological sectors, and a small path length to compensate for the low acceptance rate. In principle this recipe might allow the simulation to bypass the potential wall. In practice, with the pseudo-fermion estimate of the determinant used here, the height of the action jump at the topological sector boundary is too large and attempted crossings too frequent to allow this method to be practical. In future work, we will show that using another representation of the determinant can reduce the height of the action jump to O(1), which might make this method practical [63,64].
(2) Replace ϵ with some continuous function for small λ [39]. The substitute of the sign function will have to be broad enough so that the low eigenvalues are affected, but not too broad as this might lead to a large deviation in the final Monte Carlo ensemble. In principle, it should be possible to

10

narrow the revised ϵ as the time step decreases. One can reduce these artifacts by using a more accurate overlap operator in the accept/reject step than in the molecular dynamics [39], but this will lower the acceptance rate. Our experience with this method suggests that it cannot achieve an acceptable acceptance rate.

(3) Restrict the simulation to one topological sector, either by always reflecting (see section 4.4.2) when one encounters a potential eigenvalue crossing [65], or by using an action which suppresses small eigenvalues of the kernel operator (both by chosing a topology preserving gauge action and by adding a fermionic term) [66] . These methods have the disadvantage that one needs to calculate the re-weighting factors to combine the different topological sectors, and (more seriously) there are unresolved issues concerning whether these methods are ergodic.

(4) As soon as one encounters a crossing, one repeats the micro-canonical step, with the integration over the delta function treated exactly [26,43].

Albeit being more costly (per HMC trajectory; the situation when the auto-correlation is taken into account is unclear) than the first three approaches, method (4) is our strategy of choice as it offers best control over systematic errors from the Dirac delta function's contribution to the fermionic force, as will be explained in the following sections. Moreover, it will provide a systematic way to improve the scaling of the HMC with overlap fermions.

3.2 Computing the discontinuity

The eigenvalue crossing induces a discontinuity in the fermionic contribution to the action, the kinetic energy, and the fermionic force. From the Monte Carlo energy (4) the second equation of motion is derived imposing energy conservation:

$$\frac{dE}{d\tau} = 0 = \ldots + \Phi^\dagger \frac{d}{d\tau}\left(H^{-2}\right)\Phi. \tag{26}$$

Care needs to be taken when differentiating the fermionic contribution to the action near to a discontinuity in the overlap operator. We note that for discontinuous functions a and b, with $a = a^c(\tau) + \Delta_a \theta(\tau - \tau_c)$ and $b = b^c(\tau) + \Delta_b \theta(\tau - \tau_c)$ and a^c and b^c being continuous functions, the differential of the product of a and b is not the usual formula:

$$\frac{d}{d\tau}\left(ab\right) = \lim_{\delta\tau\to 0} \frac{1}{\delta\tau}\left[\left(a^c(\tau+\delta\tau) + \Delta_a\right)\left(b^c(\tau+\delta\tau) + \Delta_b\right) - a^c(\tau)b^c(\tau)\right]$$
$$= \lim_{\delta\tau\to 0} \frac{1}{\delta\tau}\left[\Delta_a b^c(\tau+\delta\tau) + \left(a^c(\tau+\delta\tau) + \Delta_a\right)\Delta_b\right] +$$
$$\left(a^c(\tau) + \Delta_a\right)\frac{db^c}{d\tau} + \frac{da^c(\tau)}{d\tau}b^c(\tau). \tag{27}$$

With $b = a^{-1}$, one can show that $\Delta_a b^c(\tau) + (a^c(\tau + \delta\tau) + \Delta_a)\Delta_b = 0$, and that

$$\frac{da^{-1}}{d\tau} = -a^{-1}(\tau + \delta\tau)\frac{da}{d\tau}a^{-1}(\tau).$$

Therefore,

$$\frac{d}{d\tau}H^{-2} = -\lim_{\delta\tau \to 0} H^{-2}(\tau + \delta\tau)\left.\frac{dH^2}{d\tau}\right|_\tau H^{-2}(\tau). \tag{28}$$

If there is a discontinuity in H, such as when the eigenvalue λ_1 crosses zero, then we need to take one inversion just before the crossing, leading to $X_- = H^{-2}(\lambda_1)\phi$, and the other inversion just after it, with $X_+ = H^{-2}(-\lambda_1)\phi$:

$$\frac{dE}{d\tau} = 0 = \sum_{x,\mu} \text{Tr}\left[\frac{1}{2}\frac{d}{d\tau}\Pi_\mu^2(x) - i\frac{\beta}{6}\left(\Pi_\mu(x)U_\mu(x)V_\mu(x) - h.c\right) + \right.$$
$$\left. (1 - \mu^2)\langle X_+|\left(\gamma_5\frac{d}{d\tau}\text{sign }Q + \frac{d}{d\tau}\text{sign }Q\gamma_5\right)|X_-\rangle\right]. \tag{29}$$

We denote the momenta just before and after the eigenvalue crossing as Π^- and Π^+ respectively (with the smallest eigenvalues λ_- and λ_+). We can recast equation (29) into the form

$$\frac{1}{2\delta\tau}\left[(\Pi^+)^2 - (\Pi^-)^2\right] =$$
$$-(1 - \mu^2)\langle X_+|\left(\gamma_5|\psi^l\rangle\langle\psi^l| + |\psi^l\rangle\langle\psi^l|\gamma_5\right)|X_-\rangle\frac{\epsilon(\lambda_-) - \epsilon(\lambda_+)}{\delta\tau}. \tag{30}$$

This shows that integrating over the Dirac δ function in the fermionic force will produce a discontinuity in the kinetic energy:

$$(\Pi^+)^2 - (\Pi^-)^2 = 4d(\tau_c) \tag{31}$$
$$d(\tau) = -(1 - \mu^2)\epsilon(\lambda_-)\langle X_+(\tau)|\gamma_5|\psi^l(\tau)\rangle\langle\psi^l(\tau)|X_-(\tau)\rangle$$
$$-(1 - \mu^2)\epsilon(\lambda_-)\langle X_+(\tau)|\psi^l(\tau)\rangle\langle\psi^l(\tau)|\gamma_5|X_-(\tau)\rangle. \tag{32}$$

It is straightforward to show that this discontinuity in the kinetic energy will exactly cancel the discontinuity in the pseudo-fermion action $\langle X_+|\Phi\rangle - \langle X_-|\Phi\rangle$. Therefore, energy would be conserved across the eigenvalue crossing in an exact integration. Of course, numerical integration schemes are not exact and will produce a huge error at the discontinuity. Our task is to develop an integration algorithm such as to maintain area conservation, energy conservation and reversibility in the presence of Dirac delta function forces.

4 HMC with Overlap Fermions

In this section we propose to add a correction step to the *standard leapfrog* algorithm (algorithm 1). The correction step allows us to handle the above discontinuities from eigenvalue crossing as desired. In order to realize a proper HMC scheme for overlap fermions, the correction step has to be area preserving [8] and reversible (ergodicity). In order to preserve the $O(\Delta t^2)$ complexity of the standard HMC, one must satisfy equation (29) with $O(\Delta\tau^2)$ errors or better. In the first part of this section, we shall introduce a general method suitable correction steps can be derived in a systematic manner. Thereafter, we shall present our integrator of choice, leaving the proof to appendix A that its correction step is area conserving, reversible and conserves energy with only $O(\Delta\tau^2)$ errors.

4.1 Notation

The space-time lattice is 4-dimensional with V lattice sites and $4V$ links. In general, the $SU(N_C)$ gauge group is used (although in practice, throughout this work, we will be using $N_C = 3$), so the gauge field U_τ contains a member of $SU(N_C)$ on every link, and the momentum field Π_τ is represented by a Hermitian, traceless $N_C \times N_C$ matrix on each link. The subscript τ refers to the computer time at which the gauge or momentum field is calculated. For convenience, $\Delta\tau$ is set to 1, the start of the algorithm is at time 0, so that U_0 is the original gauge field, and U_1 is the final gauge field at the end of the leapfrog correction step. $\tau_c + 1/2$ is the computer time at which the eigenvalue is 0 — the calculation of τ_c is discussed at the end of this section. The superscript "$-$" is used to indicate that the effects of the crossing are not yet included into the momentum update, and "$+$" indicates that the momentum has been updated to account for the crossing. $\Pi^+ \equiv \Pi^+_{\frac{1}{2}}$, etc., and $U_c \equiv U^-_{\frac{1}{2}+\tau_c} = U^+_{\frac{1}{2}+\tau_c}$. Finally, the notation (A, B) shall be used to represent $\sum_{x,\mu} \text{Tr}(A_\mu(x)B_\mu(x))$. The continuous part of the (Hermitian) force is $F_\tau = F^G_\tau + F^C_\tau$, with F^G and F^C defined in equations (24) and (25).

U contains an element of $SU(N_C)$ for every link, while Π is a generator of U, i.e. it contains a Hermitian, traceless $N_C \times N_C$ matrix on every link.

In order to simplify the notation for the correction step in its most general form in the following, Π is expanded in terms of an orthonormal basis. This

---

[8] We note in passing that area preservation is not a strict requirement. Non-area preserving higher-order methods will be introduced in subsequent papers which will increase the rate of transmission [61] and allow a solution to problem of mixing between low lying eigenvectors [55].

basis is defined by a set of orthonormal basis vectors which are divided into N_S subsets, $\{\{\eta_1^1, \eta_2^1, \ldots\}, \{\eta_1^2, \eta_2^2, \ldots\}, \ldots\}$. The parameter N_k gives the number of η vectors in each subset k. The η_i^k are $4V(N_C^2 - 1)$ Hermitian traceless matrices which satisfy $(\eta_i^k, \eta_j^m) = \delta_{ij}\delta^{km}$. N_k and N_S are defined such that the subscripts (i and j) run from 1 to N_k, where N_k is not necessarily constant for all the k, while the superscripts (k and m) run from 1 to N_S. For the moment, we shall leave the N_ks and N_S as arbitrary parameters, which satisfy the constraint

$$\sum_{k=1}^{N_S} N_k = 4V(N_C^2 - 1).$$

Thus, the basis is complete, so that

$$\Pi = \sum_{k=1}^{N_S} \sum_{i=1}^{N_k} \eta_i^k (\eta_i^k, \Pi). \tag{33}$$

The η matrices are functions of U_c, and are otherwise independent of the momentum. $\eta_1^1 \equiv \eta$ is defined as being normal to the gauge field surface where the eigenvalue is zero (see appendix A and equation (A.29)). η_2^1 is proportional to $F - \eta(\eta, F)$, where $F = F_{\tau_c+1/2}^+ - F_{\tau_c+1/2}^-$. The other η matrices are arbitrary.

4.2   The classical mechanics case

Before the situation of the molecular dynamics with the full overlap operator is considered, the much simpler problem of a classical mechanics particle approaching a potential wall of height $-2d$ is reviewed.

The potential energy in this case is defined as $V(q) = -2d\theta(q)$, (i.e. $V = 0$ for $q < 0$, and $V = -2d$ for $q > 0$). Note that d may be positive or negative. First, consider the one-dimensional case. The kinetic energy of the particle before it hits the wall is $\frac{1}{2}(\Pi^-)^2$. After it has hit the wall, there are two possibilities: if the initial momentum is large enough, the particle will continue onwards with a changed momentum $\Pi^+ = \sqrt{(\Pi^{-2} + 4d)}$; this case is called <u>transmission</u>. If the momentum is too small, the particle will carry insufficient kinetic energy to cross the wall and will be reflected (elastically), giving a final momentum $\Pi^+ = -\Pi^-$. This case is called <u>reflection</u>. The total energy $\frac{1}{2}\Pi^2 + V$ is of course conserved in both cases.

Next consider the classical mechanics particle in three dimensions. The coordinate system shall be defined in terms of the orthonormal basis vectors η, η_1^1, and η_2^1 as just given above. It is assumed that the potential is given by $V(\mathbf{q}) = -2d\theta((\mathbf{q}, \eta))$, such that η is the normal vector to the potential wall.

14

The three components of the momentum are defined as (Π^-, η), (Π^-, η_1^2) and (Π^-, η_2^2). It is well known what happens to the particle in classical mechanics after it hits the potential wall; in the case of transmission,

$$(\Pi^+, \eta) = \sqrt{(\Pi^-, \eta)^2 + 4d}, \tag{34}$$

is obtained, and the transverse moments are

$$(\Pi^+, \eta_i^1) = (\Pi^-, \eta_i^1). \tag{35}$$

For reflection, the final momenta will be

$$(\Pi^+, \eta) = -\,(\Pi^-, \eta),$$

and

$$(\Pi^+, \eta_i^1) = (\Pi^-, \eta_i^1), \tag{36}$$

respectively. Again, both cases conserve energy.

In fact, there is no deeper reason why the molecular dynamics trajectory must follow the classical mechanics trajectory, as long as it is energy conserving, area conserving, reversible and ergodic. One can equally well use the scheme

$$
\begin{aligned}
(\Pi^+, \eta) &= (\Pi^-, \eta) \\
(\Pi^+, \eta_i^1) &= (\Pi^-, \eta_i^1)\sqrt{1 + 4d/((\Pi^-, \eta_1^1)^2 + (\Pi^-, \eta_2^1)^2)},
\end{aligned} \tag{37}
$$

as long as it conserves the area. It is evident that this update, as well as many others which can be chosen, conserves energy. The given example also

conserves the area, as a short calculation demonstrates:

$$\left| \frac{\partial(\Pi^+, \eta_i^1)}{\partial(\Pi^-, \eta_j^1)} \right| = \begin{vmatrix} J_{11} & J_{12} \\ J_{21} & J_{22} \end{vmatrix} = 1,$$

$$J_{11} = \sqrt{1 + \frac{4d}{(\Pi^-, \eta_1^1)^2 + (\Pi^-, \eta_2^1)^2}} - \frac{4d(\Pi^-, \eta_1^1)^2}{((\Pi^-, \eta_1^1)^2 + (\Pi^-, \eta_2^1)^2)^2} \left(\sqrt{1 + \frac{4d}{(\Pi^-, \eta_1^1)^2 + (\Pi^-, \eta_2^1)^2}} \right)^{-1},$$

$$J_{12} = -\frac{4d(\Pi^-, \eta_1^1)(\Pi^-, \eta_2^1)}{((\Pi^-, \eta_1^1)^2 + (\Pi^-, \eta_2^1)^2)^2} \left(\sqrt{1 + \frac{4d}{(\Pi^-, \eta_1^1)^2 + (\Pi^-, \eta_2^1)^2}} \right)^{-1},$$

$$J_{21} = -\frac{4d(\Pi^-, \eta_1^1)(\Pi^-, \eta_2^1)}{((\Pi^-, \eta_1^1)^2 + (\Pi^-, \eta_2^1)^2)^2} \left(\sqrt{1 + \frac{4d}{(\Pi^-, \eta_1^1)^2 + (\Pi^-, \eta_2^1)^2}} \right)^{-1},$$

$$J_{22} = \sqrt{1 + \frac{4d}{(\Pi^-, \eta_1^1)^2 + (\Pi^-, \eta_2^1)^2}} - \frac{4d(\Pi^-, \eta_2^1)^2}{((\Pi^-, \eta_1^1)^2 + (\Pi^-, \eta_2^1)^2)^2} \left(\sqrt{1 + \frac{4d}{(\Pi^-, \eta_1^1)^2 + (\Pi^-, \eta_2^1)^2}} \right)^{-1}.$$

$$(38)$$

It can be shown that this latter update is reversible, since reversing the time changes $d \to -d$. Thus, instead of creating a discontinuity in the momentum *normal* to the potential wall, we are introducing the discontinuity in the directions *transverse* to the potential wall. Furthermore, one can also consider a 5-dimensional case, with two additional basis vectors η_1^2 and η_2^2, which provides the option of changing momentum in any or all of the three directions defined by η, $\{\eta_1^1, \eta_2^1\}$, and $\{\eta_1^2, \eta_2^2\}$. This general scheme will allow to achieve the $O(\Delta\tau^2)$-scalability of the approach.

4.3   The QCD situation

The are two differences in lattice QCD molecular dynamics to the classical mechanics example. Firstly, one has a considerably larger space, the configuration space of the gauge fields on the lattice. Assuming that one is working in SU(N_c), with a D-dimensional lattice, and V lattice sites, then the gauge and momentum fields exist within a $DV(N_C^2 - 1)$-dimensional space, which gives a lot of freedom in how to update the momentum fields. Secondly, a numerical integration is performed rather than an exact integration, and care must be taken as to the effects of time discretization on both the energy conservation and the area conservation.

Simple update algorithm

Now, the QCD correction update can be constructed, $(\Pi_0, U_0) \rightarrow (\Pi_1, U_1)$. The first step is to update the gauge and momentum to time $\tau + \Delta\tau/2$, as in the leapfrog procedure (algorithm 1), to yield fields Π^- and U^-:

$$
\begin{aligned}
\Pi^- &= \Pi_0 + (F_0^-)\frac{\Delta\tau}{2} \\
U^- &= e^{i\Delta\tau\Pi_-/2}U_0.
\end{aligned}
\tag{39}
$$

Next, the integration proceeds up to the crossing point itself:

$$
\Pi^-_{\frac{1}{2}+\tau_c} = \Pi^- + \tau_c F^-
\tag{40}
$$

$$
U_c = e^{i\tau_c\Pi^-}U^-.
\tag{41}
$$

We now perform the correction step. For transmission, we use equation (31):

$$
\left(\Pi^+_{\frac{1}{2}+\tau_c}, \Pi^+_{\frac{1}{2}+\tau_c}\right) = \left(\Pi^-_{\frac{1}{2}+\tau_c}, \Pi^-_{\frac{1}{2}+\tau_c}\right) + 4d.
\tag{42}
$$

In terms of our basis, a general solution of (42) [9] is

$$
\begin{aligned}
\Pi^+_{\frac{1}{2}+\tau_c} &= \Pi^-_{\frac{1}{2}+\tau_c} + \sum_{k=1}^{N_S}\left(\sum_{i=1}^{N_k}\eta_i^k(\eta_i^k, \Pi^-_{\frac{1}{2}+\tau_c})\right)\left(\sqrt{1+\frac{d_k}{\sum_i(\eta_i^k, \Pi^-_{\frac{1}{2}+\tau_c})^2}} - 1\right), \\
\sum d_k &= 4d.
\end{aligned}
\tag{43}
$$

Finally, we move back to computer time $\tau + \Delta\tau/2$, and complete the rest of the normal leapfrog integration

$$
\begin{aligned}
\Pi^+ &= \Pi^+_{\frac{1}{2}+\tau_c} - \tau_c\left(F_+\right) \tag{44} \\
U^+ &= e^{-i\tau_c\Pi^+}U_c \\
U_1 &= e^{i\Delta\tau/2\Pi^+}U^+ \\
\Pi_1 &= \Pi^+ + F_1^+\frac{\Delta\tau}{2}. \tag{45}
\end{aligned}
$$

This defines the simple update algorithm. Unfortunately we cannot make use of it because of two reasons: firstly, there is the possibility that one of the square roots in equation (43) might be imaginary (which would mean that Π would no longer be Hermitian); and secondly because the steps described in equations (40) and (44) violate detailed balance. Although τ_c is a function of the momentum, this alone is not enough to violate detailed balance, but, as shown in appendix A, an update of the momentum parallel to η will violate area conservation.

---

[9] It should be observed that this is not the most general solution: there are other possibilities involving error functions.

Maintaining detailed balance

In order to satisfy detailed balance, we can update the momentum in directions normal to η, *i.e.* we replace (40) and (44) by $\Pi^\pm_{1/2+\tau_c} = \Pi^\pm + \tau_c(F^\pm - \eta(\eta, F^\pm))$; note however that this replacement comes at the cost of an $O(\tau_c)$ violation of energy conservation. In appendix A1.1, we shall prove that a more flexible general momentum integration step which satisfies detailed balance is given by

$$
\begin{aligned}
\Pi^+ =& \Pi^- - \tau_c(F - \eta(\eta, F)) - \frac{\tau_c}{3}\mathrm{Tr}F + \eta(\eta, \Pi^-)\left(\sqrt{1 + \frac{d_1}{(\eta, \Pi^-)^2}} - 1\right) + \\
& \sum_{k=2}^{N_S}\left[\eta_1^k(\eta_1^k, \Pi^- - \frac{\tau_c}{2}(F^+ + F^-)) + \eta_2^k(\eta_2^k, \Pi^- - \frac{\tau_c}{2}(F^+ + F^-))\right] \times \\
& \left[\sqrt{1 + \frac{d_k}{[\eta_1^k, \Pi^- - \frac{\tau_c}{2}(F^+ + F^-)]^2 + [\eta_2^k, \Pi^- - \frac{\tau_c}{2}(F^+ + F^-)]^2}} - 1\right].
\end{aligned}
\tag{46}
$$

We have inserted the fermionic force dependence here for later convenience. To satisfy detailed balance, we need $N_k = 2 \ \forall k$, and the d_k should be functions only of the gauge field at the crossing and (for $k \neq 1$) (η, Π^-), and odd functions of $\Delta\tau$.

If we set $d_1 = 4d$, and $d_k = 0 \ \forall k \neq 1$, then we get an algorithm similar to that proposed in [26,43]. However, the significant disadvantage with this method — as remarked earlier — is, that it has an $O(\tau_c)$ energy conservation violating term (see appendix A.3): $\Delta E_\tau = \tau_c((F^+, \eta)(\Pi^+, \eta) - (F^-, \eta)(\Pi^-, \eta))$. This term would cripple and extremely slow down the Overlap-HMC algorithm for large lattices. In this case a much smaller time step should be applied at large volumes (as the number of correction steps increases) — rendering the HMC impractical.

Improved error behaviour

Using the just proposed general update will allow a better, $O(\Delta\tau^2)$, scaling of the energy conservation, as shown in A.3. Instead of adding $2d$ to the kinetic energy, we add $2d - \Delta E_\tau$, by setting $\sum d_k = 4d - 2\Delta E_\tau$. We can also remove some (though not all) of the $O(\Delta\tau^2)$ error in the same way, leaving us with errors which are close to $O(\Delta\tau^3)$, as demonstrated numerically in section 5.1.2. The presence of $O(\Delta\tau^2)$ errors is not inconsistent with reversibility because τ_c is an even function of $\Delta\tau$.

These are the most important improvements of our method over that proposed in [26,43].

Transmission and reflection

A further problem arises when one of the square roots in equation (46) becomes imaginary. In analogy to the classical mechanics picture discussed above, following [26,43], we reflect off the $\lambda = 0$ surface. On the one hand, if the momentum is large enough, then we pass through into the new topological sector with a changed momentum. As in the classical mechanics example, we call this case *transmission*, [10] and this is the scenario described so far in this section. On the other hand, if the momentum is too small, we bounce off the $\lambda = 0$ surface. As before, this is denoted as *reflection*. Unlike transmission, a reflection update is accompanied neither with a change in topological index nor with a discontinuity in the fermionic action.

Still there is a further subtlety which needs to be addressed before one can formulate the algorithms for transmission and reflection. With the techniques used in this article, the combined update step should also be area conserving. As an example, suppose that we set $d_1 = 4d$, and all the other $d_k = 0$, and we reflect whenever $1 + \frac{4d}{(\eta, \Pi^-)^2} < 0$. The method by which we choose to reflect or transmit is denoted as the *reflection condition*. One can write:

$$\Pi^+ = \Pi^{+\text{transmission}}\theta\left(1 + \frac{4d}{(\eta, \Pi^-)^2}\right) + \Pi^{+\text{reflection}}\left(1 - \theta\left(1 + \frac{4d}{(\eta, \Pi^-)^2}\right)\right).$$
(47)

When calculating the Jacobian one must differentiate the θ (step) functions, which might lead to a Jacobian of the form $1 - \delta(1 + 4d/(\eta, \Pi^-)^2)$. This issue is outlined in more detail in appendices A.2.3 and A.2.4. In these appendices we demonstrate that the δ-function is not present if the reflection condition is independent of the momentum (i.e. we reflect when $|d| > d_{max}$), or if there is no discontinuity between the transmission and reflection updates. We also argue in the appendices that even if the δ−function is present in the Jacobian, it will not affect the final ensemble. We test this conclusion numerically in section 5.4. Both theoretically and in the numerical experiment, no systematic error is found.

4.4 Integration over the discontinuity

A first approximation of τ_c can be determined by a Taylor expansion of the eigenvalue around zero (see equation (17)):

$$\tau_c = -\frac{\langle \psi^l | Q | \psi^l \rangle}{\langle \psi^l | \dot{Q} | \psi^l \rangle}.$$
(48)

---

[10] It is called *refraction* in [26,43]

This gives the correct value of τ_c up to order τ_c^2. We can, in principle, calculate τ_c using (48) from either the gauge field U^+ or the gauge field U^-. There will be a small deviation between the two calculations, and therefore a small discrepancy between d and η calculated from the two gauge fields. This will lead to a breakdown in reversibility if we apply algorithm 2 naively. There are two possible ways in which this problem can be overcome. Firstly, one can calculate τ_c from U^- if $\tau_c/\Delta\tau < 0$ (i.e. we have already passed the crossing at molecular dynamics time $\tau + \Delta\tau/2$), and use U^+ to calculate τ_c otherwise. Calculating τ_c using U^+ requires an iterative procedure; we used a combination of simple iteration and the Van Wijngaarden-Dekker-Brent (VWDB) method [67,68] for root finding, which was reasonably effective. The second, and our preferred, possibility is to calculate τ_c exactly using a root finding algorithm, such as either Newton-Raphson or VWDB. We used a Newton-Raphson algorithm, iterating

$$\tau_c^n = \tau_c^{n-1} - \frac{\langle \psi^l(\Delta\tau/2 + \tau_c^{n-1})|Q(\Delta\tau/2 + \tau_c^{n-1})|\psi^l(\Delta\tau/2 + \tau_c^{n-1})\rangle}{\langle \psi^l(\Delta\tau/2 + \tau_c^{n-1})|\dot{Q}(\Delta\tau/2 + \tau_c^{n-1})|\psi^l(\Delta\tau/2 + \tau_c^{n-1})\rangle}, \quad (49)$$

so that we could improve the accuracy of the eigenvector as the Newton-Raphson iteration progressed. The difficulty with bounded methods such as bisection or VWDB is that trying to constrain the eigenvector between two bounds could lead to a high accuracy eigenvector escaping bounds calculated with a low accuracy. Using Newton-Raphson allows us to adjust the accuracy of the eigenvector as we proceed with the calculation. This method, of finding the exact point where the eigenvalue crosses, has the advantage that it removes one source of $O(\Delta\tau^2)$ energy conservation violating terms, and it also was faster than the simple iterative method on our small trial lattices. However, the eigenvector with the smallest eigenvalue needs to be calculated to a very high accuracy. This method breaks down if the crossing is close to a minimum of the eigenvalue. In this case, it is necessary to use a different algorithm, such as Brent's method, to get sufficiently close enough to the solution for Newton-Raphson to converge.

4.4.1 Transmission

The update scheme proposed for transmission is given by (see algorithm 2):

$$\Pi^+ = \Pi^- + \tau_c(F) - \eta\tau_c(\eta, F) - \frac{\tau_c}{3}\mathrm{Tr}(F) +$$
$$\left(\eta_1^k(\eta_1^k, \Pi^- - \frac{\tau_c}{2}(F^- + F^+)) + \eta_2^k(\eta_2^2, \Pi^- - \frac{\tau_c}{2}(F^- + F^+))\right) \times$$
$$\left(\sqrt{1 + \frac{d_k}{(\eta_1^k, \Pi^- - \frac{\tau_c}{2}(F^- + F^+))^2 + (\eta_2^k, \Pi^- - \frac{\tau_c}{2}(F^- + F^+))^2}} - 1\right)$$

$$ (50)$$

$$d_k = \frac{1}{N_S}(4d - 2\tau_c(F^-, \eta)(\Pi^-, \eta) + 2\tau_c(F^+, \eta)(\Pi^+, \eta) + \tau_c^2(F^- + F^+, F^+ - F^-)).$$

As mentioned earlier, η_1^k, and η_2^k must be orthonormal and orthogonal to η and F. We constructed these vectors using the following procedure:

- We start by taking three unit vectors, α, β and γ corresponding to putting one of the eight Gell-Mann matrices on one particular link.
- We then construct $\eta_1^k = \alpha\cos\theta + \beta\sin\theta\cos\phi + \gamma\sin\theta\sin\phi$, choosing the angles θ and ϕ so that η_1^k is normal to η and F.
- η_2^k is then constructed in the same way from three different Gell-Mann matrices on the same link.

Therefore N_S is the number of links on the lattice. It should be noted that this procedure does not lead to a higher transmission rate than other choices.[11] The change of momentum for any pair of $\eta-$vectors is proportional to $1/N_S$, but there are N_S pairs of vectors, so the overall probability of transmission remains constant. Indeed, we will show in a forthcoming paper [61] that (if we are updating the momentum normal to η and assuming that Π is Gaussian distributed) the probability of transmission is always $\min(1, \exp(-\frac{1}{2}\sum d_k)) + O(1/V)$, no matter which area-conserving algorithm is chosen. We investigate below how this choice of transmission algorithm will affect the numerical stability and the transmission rate.

4.4.2 Reflection

A reflection takes place whenever one of the momentum updates in the transmission algorithm would lead to an imaginary momentum. To correct for the reflection's $O(\tau)$ errors, one can use a method similar to the one which we use for transmission. Indeed, we used this algorithm for a while, and it worked

---

[11] Although it is possible to use non-area conserving algorithms with a higher transmission rate — see [61].

(1) $\Pi^-(\tau + \Delta\tau/2) = \Pi(\tau) + \Delta\tau/2\dot{\Pi}(\tau)$;
(2) $U^-(\tau + \Delta\tau/2) = e^{i(\Delta\tau/2)\Pi^-(\tau+\Delta\tau/2)}U(\tau)$;
(3) $U_c = e^{i\tau_c\Pi^-}U^-$;
(4) The momentum update given in equation 50;
(5) $U^+ = e^{-i\tau_c\Pi^+}U_c$;
(6) $U(\tau + \Delta\tau) = e^{i(\Delta\tau/2)\Pi^+(\tau+\Delta\tau/2)}U^+(\tau + \Delta\tau/2)$;
(7) $\Pi(\tau + \Delta\tau) = \Pi^+(\tau + \Delta\tau/2) + (\Delta\tau/2)\dot{\Pi}_+(\tau + \Delta\tau)$.

Algorithm 2. The modified leapfrog algorithm for transmission.

(1) $\Pi^-(\tau + \Delta\tau/2) = \Pi(\tau) + (\Delta\tau/2)\dot{\Pi}(\tau)$;
(2) $U^-(\tau + \Delta\tau/2) = e^{i(\Delta\tau/2)\Pi^-(\tau+\Delta\tau/2)}U(\tau)$;
(3) $U_c = e^{i\tau_c\Pi^-}U^-$;
(4) The momentum update given in equation (51);
(5) $U^+ = e^{i\tau_c\Pi^+}U_c$;
(6) $U(\tau + \Delta\tau) = e^{i(\Delta\tau/2)\Pi^+(\tau+\Delta\tau/2)}U^+(\tau + \Delta\tau/2)$;
(7) $\Pi(\tau + \Delta\tau) = \Pi^+(\tau + \Delta\tau/2) + (\Delta\tau/2)\dot{\Pi}_+(\tau + \Delta\tau)$.

Algorithm 3. The modified leapfrog algorithm for reflection.

well. However, there remains a problem with this method, which is what to do when the O(τ_c) error becomes sufficiently large that the square roots in the O(τ_c) correction become imaginary. Although this scenario did not occur in practice, it is a worrying possibility with no obvious answer. We have subsequently switched to a method first proposed by Fodor *et. al.* [65], which is based around a different idea. Our current update for reflection (see algorithm 3) is

$$\Pi^+ = \Pi^- - 2\eta(\eta, \Pi^-) - 2\tau_c(F^-) + 2\eta\tau_c(\eta, F^-) + 2\frac{\tau_c}{3}\text{Tr}(F^-). \qquad (51)$$

Note the change of sign in the gauge field update in step (5) of algorithm 3, as compared to algorithm 2.

The sign of the smallest eigenvalue should change for a transmission step, and remain the same for reflection. However on a few rare occasions, this did not occur. Such odd phenomena happen if the $\lambda = 0$ surface is not smooth near to the point of crossing, so that the eigenvalue might try to cross again in the same molecular dynamics step. We corrected for this by adding a second correction step (i.e. we repeated steps (3) (4) and (5)) if the sign of the smallest eigenvalue did not behave as expected.

Two different eigenvalues crossing during the same micro-canonical step will also cause this algorithm to break down, because of possible mixing between the two eigenvectors. This issue is discussed in appendix B. This phenomenon will be discussed in a future paper [55].

5 Numerical Results

In order to test the overlap HMC algorithm numerically on various small lattices, 4^4, $N_F = 2$ ensembles with $\beta = 5.4$ were generated, one set of runs with parameter settings $\kappa = 0.225$ and $\mu = 0.05, 0.1, 0.2, 0.3, 0.4$ and 0.5, the other with $\mu = 0.5$ and $\kappa = 0.18, 0.19, 0.2, 0.21, 0.22$ and 0.23. We have also generated three 6^4, $\beta = 5.6$ ensembles, with $\kappa = 0.2$ and $\mu = 0.3, 0.1, 0.05$, and two 8^4, $\beta = 5.6$ ensembles at $\kappa = 0.2$, and $\mu = 0.1$ or 0.3, although we did not analyse the small statistics 8^4 data sets for most of the results presented in this section. Phenomenological calculations using the overlap operator in the quenched approximation have covered masses in the range $\mu \sim 0.007 \rightarrow 0.4$ [24] or $\mu \sim 0.015 \rightarrow 0.037$ [69], roughly a factor of 10 below our present mass range. [12] Throughout these simulations, we took advantage of relaxation and preconditioning techniques developed in [46,47]. The accuracy of the preconditioner and the number of projected eigenvalues were optimised for our HMC program, which gave a gain factor of ~ 30. We used anti-periodic boundary conditions in the time direction and periodic boundary conditions in the spatial directions.

5.1 *Energy conservation and topological index*

5.1.1 *The correction step and the number of topological index changes*

Our first concern is to verify the impact of the correction step on energy conservation, *i.e.* on the size of energy fluctuations during a Monte Carlo run. This can be achieved by a comparison of the upper plots of figures 1 and 2, which display the energy variations during the individual trajectories for a typical run. The lower plots in these figures exhibit the tunnelling histories of the systems through the topological sectors. A large spike in the energy difference signals a breakdown in energy conservation. Without the correction step (figure 1) there are spikes in the energy difference whenever the topological charge changes — which occurs when there is an eigenvalue crossing. This confirms our expectation that energy is not conserved when the topological index changes if the standard leapfrog algorithm is used. In all subsequent plots, we shall use *the corrected update*. Figure 2 is based on the same pa-

---

[12] In order to express μ as a physical mass, we used $r_0 = 0.49$fm to calculate the lattice spacing as approximately $a^{-1} \sim 590$MeV on our 6^4 lattices. The renormalisation constant was not possible to measure on these lattices because the error was too large, so, for this rough estimate, we will take $Z_m = 1$. This implies that on these ensembles a quark mass of $\mu = 0.05$ corresponds to a physical mass of ~ 93 MeV, *i.e.* around the value of the strange quark mass, however with a very large error.
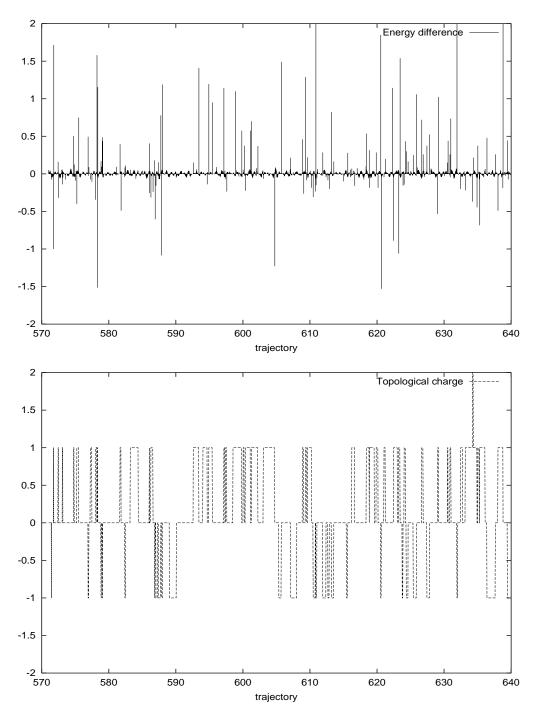
Fig. 1. The energy difference between two micro-canonical steps, and the topological index plotted against the trajectory number, for a $\beta = 5.4$, $\mu = 0.5$, $\kappa = 0.225$ ensemble generated without the correction step.

rameters as figure 1; generally we find that most of the spikes disappear. The remaining spikes are caused when a positive and a negative eigenvalue of Q both approach, but do not cross, 0 simultaneously. This can cause large mixing between the two eigenvectors, and a very large fermionic force. This second
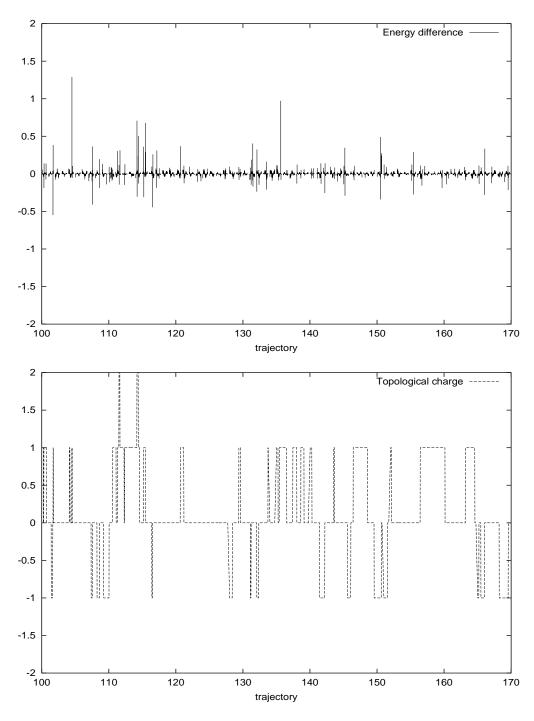
Fig. 2. The energy difference between two micro-canonical steps and the topological index plotted against the trajectory number for 70 trajectories of the $\beta = 5.4$, $\mu = 0.5$, $\kappa = 0.225$ ensemble, generated with the correction step.

effect will not affect the acceptance rate. It should be noted that sometimes the topological index bounces back within the same time step, which can cause a small discontinuity in the energy (unless, like our code, the HMC algorithm is designed to pick up this possibility).
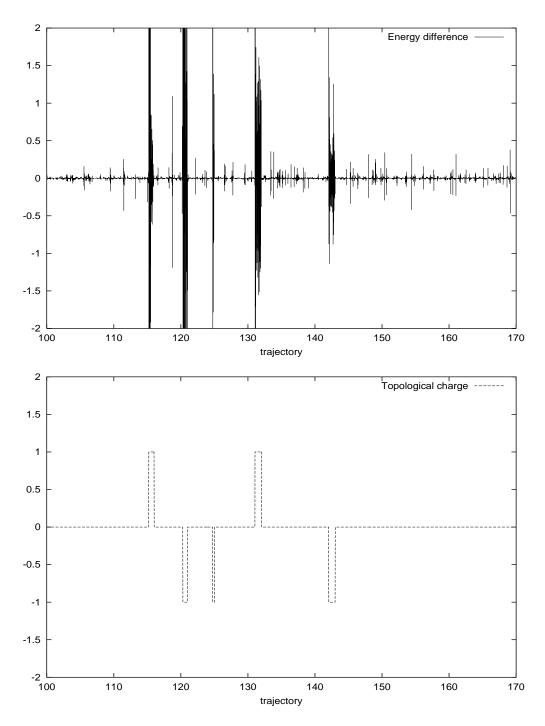
25

Fig. 3. The energy difference between two micro-canonical steps (top), and the topological index (bottom) plotted against the trajectory number for 70 trajectories of the $\beta = 5.4$ $\mu = 0.05$ $\kappa = 0.225$ ensemble. We used the correction step to generate this ensemble.

4^4	$\mu = 0.5$	4^4	$\kappa = 0.225$	6^4	$\kappa = 0.2$	8^4	$\kappa = 0.2$
κ	n_{top}	μ	n_{top}	μ	n_{top}	μ	n_{top}
0.18	0.000(0)	0.05	0.045(12)	0.05	0.040(14)		
0.19	0.006(6)	0.1	0.103(20)	0.1	0.074(18)	0.1	0.153(42)
0.2	0.122(31)	0.2	0.393(39)				
0.21	0.579(30)	0.3	0.567(46)	0.3	0.547(74)	0.3	0.969(175)
0.22	0.901(104)	0.4	0.827(52)				
0.23	1.21(83)	0.5	1.12(73)				

Table 1

The number of topological index changes per trajectory (n_{top}) for various masses on our 4^4, $\kappa = 0.225$ ensembles (left), the 4^4, $\mu = 0.5$ ensembles (middle), and the 6^4, $\kappa = 0.2$ ensembles (right). Note that the 4^4 and 6^4 ensembles were generated at different values of κ (and β), so the bare quark mass at constant μ is 20% lower for the 6^4 ensembles.

When we go down to smaller masses, a slightly different picture emerges (see figure 3 — note that this figure includes the correction step). We notice that the topological index, Q_f, changes considerably less frequently at a lower mass (see table 1, 2nd-4th columns), as we would expect. The $Q_f \neq 0$ configurations are suppressed as we move to lower masses, and as the mass decreases, d increases, [13] leading to a lower probability of transmission. [14] The energy difference depends strongly on the topological index: on the 4^4, $\mu = 0.05$ ensembles, the mass is about the same size as the lowest non-zero eigenvalue, implying that the inverse of the overlap operator, and therefore in general the fermionic force, will be larger for a $Q_f \neq 0$ configuration. We have only observed this effect of the large fermionic forces with non-trivial topology on our smallest lattices, although it is possible that it will return in large volumes in the ϵ-regime. It can be avoided by working in the chiral sector with no zero modes [39,61].

Finally, it can be seen that reducing κ (and therefore reducing the Wilson mass m_0 and as a consequence the bare fermion mass) generally reduces the number of crossings (see figure 4 and table 1 (first column)). As expected, see [70,71], there are no changes in the topological index below the critical value of κ, which is around 0.2 on the 4^4 lattices. We confirm that the overlap operator has very few small eigenvalues below the critical value of κ [72].

---

[13] More precisely $d \propto \mu^{-2}$.

[14] The probability of transmission is proportional to $\min(1, \exp(-2d))$.
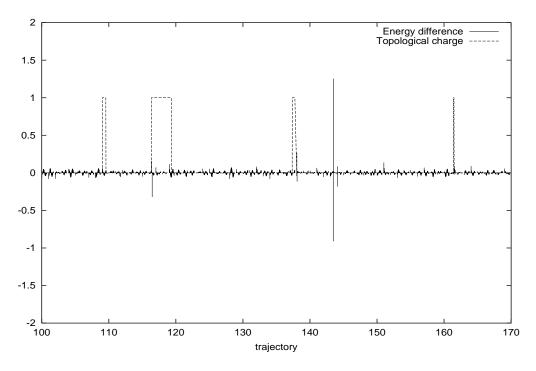
Fig. 4. The energy difference between two micro-canonical steps, and the topological index plotted against the trajectory number for a section of the $\beta = 5.4$ $\mu = 0.5$ $\kappa = 0.2$ ensemble.

5.1.2 Complexity of correction step

To investigate the $\Delta\tau$ dependence of the energy conservation violation for the correction step, we took 100 6^4, $\mu = 0.3$ configurations, containing 35 transmission correction steps and 123 reflection correction steps. We ran the molecular dynamics as normal (with $\Delta\tau = 1/30$) up to the eigenvalue crossing. We then reduced the time step for the molecular dynamics to $\Delta\tau/n_t$, running $n_t - 1$ normal leapfrog updates and one modified leapfrog update. We calculated the absolute value of the error in the energy for the modified leapfrog step only and averaged over the configurations. This procedure ensures that on each configuration the gauge field and momentum at the crossing have only a small dependence on n_t. The energy differences for our procedures (algorithm 2) and the algorithm proposed in [26,43] are given in tables 2 for the transmission step and 3 for the reflection step. We expect (see appendix A.3) an $O(\tau_c)$ error for the algorithm proposed in [26,43] and an $O(\tau_c^2)$ error for the algorithm presented in this paper, where $-\Delta\tau/(2n_t) < \tau_c < \Delta\tau/(2n_t)$. Fitting the results to the form $a_0 n_t^{a_1}$ gave the results as presented in table 4.

First, consider the results for the algorithm presented in [26,43]. Comparing the raw data with $\Delta\tau$ and $\Delta\tau^2$ in tables 2 and 3 suggests that the energy conservation is dominated by $O(\Delta\tau)$ terms. This is also indicated by the results of the fits in table 4. Furthermore, $\Delta E_0/\tau_c$ is large and constant (there are still some large contributions from the standard leapfrog part of our algorithm

28

| | | | [26] | | | section 4 | | |
n_t	$1/n_t$	$1/n_t^2$	$|\Delta E_0|$	$\frac{\Delta E_0}{\Delta E_0(n_t=1)}$	$\Delta\tau\frac{\Delta E_0}{\tau_c}$	$|\Delta E|$	$\frac{\Delta E}{\Delta E(n_t=1)}$	$\Delta\tau\frac{\Delta E}{\tau_c}$
1	1.000	1.000	0.120(21)	1.000(172)	0.50(9)	0.059(6)	1.000(105)	0.83(33)
2	0.500	0.250	0.050(9)	0.414(76)	0.37(5)	0.009(1)	0.154(25)	0.14(4)
3	0.333	0.111	0.031(7)	0.261(57)	0.32(5)	0.0030(7)	0.051(12)	0.16(8)
4	0.250	0.063	0.019(4)	0.154(32)	0.31(4)	0.0016(4)	0.027(7)	0.21(14)
5	0.200	0.040	0.015(3)	0.122(27)	0.31(5)	0.0009(2)	0.015(3)	0.032(8)
6	0.167	0.028	0.013(3)	0.107(27)	0.35(6)	0.0005(1)	0.008(2)	0.018(4)
7	0.143	0.020	0.011(2)	0.090(19)	0.34(5)	0.0004(1)	0.007(2)	0.019(4)

Table 2

The energy difference ΔE for the transmission correction algorithm 2 compared with the molecular dynamics time step, $\Delta\tau = 1/30 n_t$. For comparison, results for the algorithm given in [26], here denoted as ΔE_0, are also included.

| | | | [26] | | | section 4 | | |
n_t	$1/n_t$	$1/n_t^2$	$|\Delta E_0|$	$\frac{\Delta E_0}{\Delta E_0(n_t=1)}$	$\Delta\tau\frac{\Delta E_0}{\tau_c}$	$|\Delta E|$	$\frac{\Delta E}{\Delta E(n_t=1)}$	$\Delta\tau\frac{\Delta E}{\tau_c}$
1	1.000	1.000	0.296(30)	1.000(101)	1.35(12)	0.105(23)	1.000(215)	0.94(23)
2	0.500	0.250	0.133(13)	0.451(44)	1.16(10)	0.0114(30)	0.109(28)	0.16(3)
3	0.333	0.111	0.099(11)	0.335(37)	1.12(9)	0.0030(5)	0.028(4)	0.08(2)
4	0.250	0.063	0.064(7)	0.217(25)	1.16(10)	0.0027(16)	0.026(2)	0.08(2)
5	0.200	0.040	0.059(6)	0.198(19)	1.16(9)	0.0011(4)	0.011(4)	0.07(3)
6	0.167	0.028	0.045(5)	0.151(16)	1.12(9)	0.00049(9)	0.005(1)	0.03(1)
7	0.143	0.020	0.036(4)	0.123(14)	1.12(9)	0.00037(8)	0.004(1)	0.06(2)

Table 3

The energy difference ΔE for the reflection correction algorithm 2 compared with the molecular dynamics time step, $\Delta\tau = 1/30 n_t$. For comparison, results for the algorithm given in [26], here denoted as ΔE_0, are also included.

	a_0	a_1	χ^2
ΔE_0 ([26])	$0.119(^{+0.027}_{-0.026})$	$-1.271(^{+0.183}_{-0.173})$	0.52
ΔE (section 4)	$0.058(^{+0.009}_{-0.009})$	$-2.642(^{+0.137}_{-0.139})$	1.11
ΔE_0 ([26])	$0.291(^{+0.037}_{-0.036})$	$-1.044(^{+0.094}_{-0.092})$	0.92
ΔE (section 4)	$0.083(^{+0.029}_{-0.026})$	$-2.879(^{+0.266}_{-0.245})$	4.01

Table 4

Fits and χ^2 values for the data presented in tables 2 and 3 for the functional form $\Delta E = a_0 n_t^{a_1}$ for transmission (top) and reflection (bottom). The errors are the 68% confidence levels for the fit.

at $n_t = 1$), suggesting that the violation in energy conservation is dominated by a large $O(\tau_c)$ term. For the energy differences given by our algorithm, a different picture emerges: the violation in energy conservation is dominated by the $O(\Delta\tau^3)$ terms from the normal leapfrog part (steps 1, 2, 6 and 7) of the algorithm, while the $O(\tau_c^2)$ error which we expect from the correction steps (steps 3-5 in algorithm 2) is small. This is an encouraging result that deserves to be investigated on larger lattices and smaller masses.

μ	$<S_g>$	τ_j	P_l	κ	$<S_g>$	τ_j	P_l
0.05	0.5754(10)	$25.05(^{+32.57}_{-12.63})$	-0.0716(40)	0.18	0.5485(14)	$6.31(^{+1.66}_{-1.30})$	-0.0137(31)
0.1	0.5733(7)	$12.76(^{+4.07}_{-4.71})$	-0.0778(51)	0.19	0.5522(8)	$3.77(^{+0.71}_{-0.59})$	-0.0153(58)
0.2	0.5678(14)	$11.90(^{+4.36}_{-3.21})$	-0.0506(61)	0.2	0.5555(10)	$6.71(^{+1.55}_{-1.21})$	-0.0054(50)
0.3	0.5638(8)	$4.60(^{+3.19}_{-1.94})$	-0.0376(55)	0.21	0.5573(8)	$1.82(^{+0.71}_{-0.54})$	-0.0241(80)
0.4	0.5570(9)	$3.98(^{+0.74}_{-0.62})$	-0.0223(65)	0.22	0.5560(11)	$1.88(^{+2.14}_{-1.88})$	-0.0266(94)
0.5	0.5523(13)	$4.46(^{+0.77}_{-0.94})$	-0.0050(80)	0.23	0.5528(14)	$5.26(^{+1.36}_{1.08})$	-0.0015(69)

Table 5

The average gauge energy per lattice site, $<S_g>$, the real part of the Polyakov loop P_l and jackknife auto-correlation lengths for the plaquette, for the 4^4, $\kappa = 0.225$ ensembles (left) and the $\mu = 0.5$ ensembles (right).

5.2   Polyakov loop and plaquette

Next we calculate several observables to check that we get sensible numbers. Here we look at the value of the plaquette—or, equivalently, the average gauge energy per lattice site, $S_g = \left\langle 1 - \frac{1}{2N_C}(U_{\mu\nu} + U_{\mu\nu}^\dagger) \right\rangle$ — and the real part of the Polyakov loop.

The values of the gauge energy per lattice site and the Polyakov loop for one of our ensembles are plotted against computer time in figure 5 (other ensembles are similar). Both the plaquette and the Polyakov loop are stable over computer time. The average Polyakov loop, given in tables 5 and 6 is small for all our configurations, suggesting that the configurations are all confined. The average value of S_g per lattice site is given in tables 5 and 6. The statistical errors on S_g shown in these tables were obtained by calculating the jackknife error $\sigma_j^{(n_j)}$ with n_j consecutive configurations in each bin. The jackknife method should give a stable value when $n_j \gg \tau_i$, the auto-correlation length. By fitting the jackknife errors to the curve $\sigma_j^{(n_j)} = a + b(1 - e^{-n_j/\tau_j})$ (the errors on $\sigma_j^{(n_j)}$ were calculated using the bootstrap method) we can get an estimate of the value of the plateau ($\sigma_j = a + b$), and a measure, τ_j, of the exponential auto-correlation length. On the 4^4 lattices, the auto-correlation length is small at the larger masses, but increases roughly as $1/\mu$ as we decrease the mass. On the larger lattices, the auto-correlation time is more stable with the mass. We were not able to obtain a reliable estimate of the integrated auto-correlation times on such small lattices.

5.3   Topological susceptibility

The average values of the topological index, $Q_f = n_- - n_+$ ($n_\pm$ is the number of positive/negative chirality zero modes), and of Q_f^2 are given in tables 7 and 8 and are plotted in figure 6. The tables show that the average values of Q_f are generally close to 0, suggesting that there is no bias towards either a positive
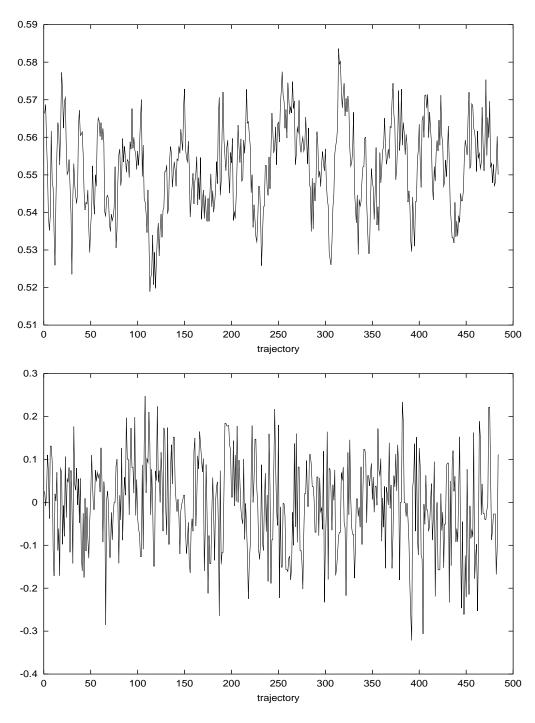
Fig. 5. The gauge energy per lattice site (top) and Polyakov loop (bottom) for each trajectory on the 4^4 , $\mu = 0.5$, $\kappa = 0.225$ ensemble.

or negative topological index.

The topological susceptibility, which is proportional to $< Q_f^2 >$, can be related to the quark mass using chiral perturbation theory [73,74,75]. It is expected that at low quark masses on large enough volumes the topological susceptibil-

μ	$< S_g >$	τ_j	P_l
0.05	0.5353(10)	$9.97(^{+1.71}_{-1.48})$	-0.0082(48)
0.1	0.5350(6)	$8.59(^{+0.79}_{-0.62})$	-0.0049(33)
0.3	0.5230(19)	$10.93(^{+2.73}_{-2.18})$	-0.0018(28)

Table 6

The average gauge energy per lattice site, $< S_g >$, the real part of the Polyakov loop P_l and jackknife auto-correlation lengths for the 6^4 ensembles.

μ	m_b	$< Q_f^2 >$	$< Q_f >$	n_{conf}	κ	$< Q_f^2 >$	$< Q_f >$	n_{conf}
0.05	0.19	0.019(6)	$-0.011(5)$	734	0.18	0.000(0)	0.000(0)	459
0.1	0.40	0.118(18)	0.021(33)	959	0.19	0.003(4)	0.004(4)	733
0.2	0.89	0.343(36)	0.044(34)	868	0.2	0.044(16)	$-0.001(14)$	760
0.3	1.52	0.421(41)	$-0.085(35)$	967	0.21	0.255(35)	0.014(41)	442
0.4	2.37	0.507(46)	0.034(39)	905	0.22	0.461(44)	$-0.047(62)$	706
0.5	3.56	0.480(62)	0.057(47)	523	0.23	0.667(89)	0.088(66)	433

Table 7

The average values of the topological index Q_f, Q_f^2, and the number of configurations for the 4^4, $\kappa = 0.225$ ensembles(left) and the 4^4, $\mu = 0.5$ ensembles (right). m_b is the bare fermion mass, given by equation (10).

ity should be proportional to the quark mass, the square of the pion mass:

$$\chi = \frac{< Q_f^2 >}{V} \sim \frac{f_\pi^2 m_\pi^2}{2N_F} + O(m_\pi^4). \tag{52}$$

There have been several attempts to verify this relation in recent years (for recent examples, see [76,77]), with mixed success. At larger quark masses, the topological susceptibility should tend asymptotically towards its quenched value. The transition between the two forms, in a large volume, is expected to be around 50-90 MeV [78]. Our bare quark masses, which we estimate (based on our early calculations of the lattice spacing on our 6^4 ensembles) range from about 100 MeV to a few GeV and should be in the transitional region between the two known limits: we cannot expect to see a linear decrease with the quark mass. However, we recognize a decrease in the topological susceptibility, and our results are not inconsistent with the expected functional form, although again we emphasise that our lattices are far too small to draw any meaningful conclusions.

μ	m_b	$< Q_f^2 >$	$< Q_f >$	n_{conf}
0.05	0.19	0.063(21)	$-0.008(21)$	377
0.1	0.40	0.138(22)	0.026(20)	350
0.3	1.52	0.493(62)	0.086(61)	420

Table 8
The average values of the topological index Q_f, Q_f^2, and the number of configurations for the 6^4 ensembles. m_b is the bare fermion mass.

condition	n_{conf}	AR	n_{top}	$< Q_f^2 >$	$< S_g >$	$< P_l >$
$|d| > 0.5$	709	81.9%	1.048(68)	0.354(35)	0.5625	-0.0325
$|d| > 0.45$	855	84.1%	0.978(57)	0.326(26)	0.5653	-0.0286
$|d| > 0.4$	864	86.2%	0.920(60)	0.317(33)	0.5640	-0.0377
$|d| > 0.35$	460	86.5%	0.843(74)	0.350(33)	0.5645	-0.0270
$|d| > 0.3$	705	87.8%	0.688(59)	0.311(35)	0.5646	-0.0300
$|d| > 0.25$	698	92.0%	0.598(50)	0.317(34)	0.5657	-0.0431
$|d| > 0.2$	604	96.0%	0.439(55)	0.285(31)	0.5653	-0.0353
$1 + \dfrac{d_2}{\sum_k (\eta_k^2, \Pi_-)^2} > 0$	768	97.8%	1.047(62)	0.357(32)	0.5639	-0.0357

Table 9
The acceptance rate, number of topological index changes per trajectory, n_{top}, and average values of Q_f^2, S_g and P_l for 4^4 ensembles generated at $\mu = 0.3$, $\kappa = 0.225$ and $\beta = 5.4$, but with different reflection conditions.

5.4 Testing the area conservation of the reflection condition.

As remarked earlier, the reflection condition applied is to be tested numerically in order to verify that area conservation is fulfilled and no systematic errors are spoiling the results. We compared the results from our algorithm with the results from a second algorithm which explicitly satisfies detailed balance, but where the molecular dynamics does not always conserve energy. This algorithm reflected whenever d was smaller than a constant d_{max} and used no correction step for transmission. When d was larger than this constant, it violated energy conservation. A high $d_{\max}$ leads to many topological index changes and therefore a short topological auto-correlation length but has a low acceptance rate. A low $d_{\max}$ would have a higher acceptance rate but fewer topological index changes.

In table 9, we show how a varying $d_{\max}$ affects the acceptance rate and the number of topological index changes per trajectory. Using the exact area-conserving algorithm has a cost in either the acceptance rate or rate of topological charge changes. Setting $d_{max} = 0.5$ has a similar number of topological index changes per trajectory, but at a cost of 15% in the acceptance rate. Lowering d_{max} so that the acceptance rate is similar to the momentum-dependent algorithm reduces the number of topological index changes by over a factor of
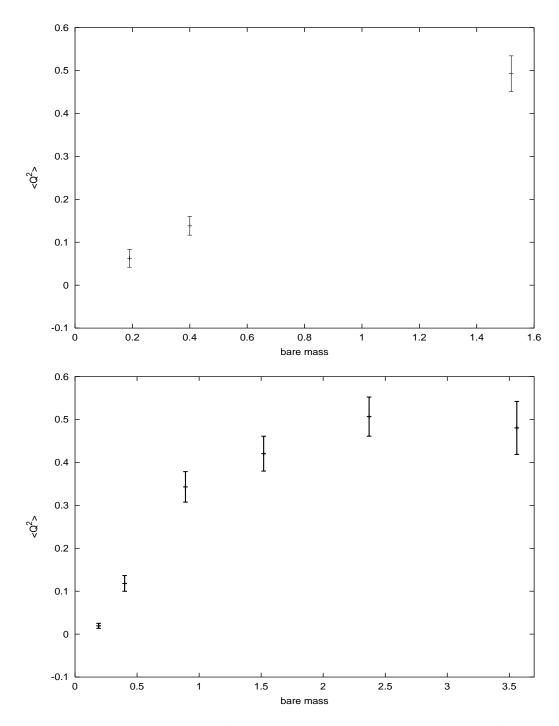
Fig. 6. The ensemble average of Q_f^2 plotted against bare quark mass on the 6^4 (top) and 4^4 (bottom) ensembles.

2, and increases the auto-correlation correspondingly.

The table shows that the average values of plaquette, topological susceptibility and Polyakov loop are independent of the reflection condition. We therefore feel confirmed in assuming that a potential systematic error is extremely small.

However, this issue will need to be checked again when we move to larger lattices at smaller masses.

5.4.1 Volume scaling of the overlap HMC

The authors of Ref. [57] remark that the algorithm might scale with the square of the lattice volume. Their argument goes as follows:

(1) The density of small eigenvalues should be independent of the volume; therefore the number of small eigenvalues scales with the volume.
(2) The number of Wilson eigenvalues attempting to cross the zero line will be proportional to the density of small eigenvalues. Therefore, there will be $O(V)$ correction steps. [15]
(3) In total, the algorithm might scale as V^2.

There are, however, arguments against this reasoning: The density of small eigenvalues is not just a function of the lattice volume as point (2) suggests, but also the lattice spacing and the fermion mass. Thus, concluding that the number of correction steps will be proportional to the volume is too simplistic, as on larger volumes we are also likely to change the other parameters in the action. One could use the same argument to suggest that the algorithm will accelerate as the lattice spacing decreases, since there will be fewer attempted crossings. More importantly, this argument does not take into account the effect of the auto-correlation. Our numerical experience shows that the overlap eigenvalues are remarkably stable under the molecular dynamics, except when there is a topological index change. Our results [80] demonstrated that small non-zero eigenvalues of the overlap operator are only generated significantly faster through the mechanism of two topological index changes rather than the normal evolution of the molecular dynamics. Thus the auto-correlation time depends strongly on the rate of topological index changes, which in turn, assuming that the transmission rate is large enough, increases proportional to the rate of attempted eigenvalue crossings. Thus the more attempted topological index changes, the shorter the auto-correlation times should be.

Nonetheless, we expect problems with the condition number of both the overlap and Wilson operators increasing as the volume increases, leading to a slowing down in both the eigenvalue and inversion routines.

Results from test runs on lattices ranging from size 4^4 to $16^3 32$ show that the number of required correction steps is certainly not proportional to the volume; still it is increasing slightly.

---

[15] See the results of [79]; we are intending to test these results.

μ	Time	n_{md}	AR	κ	Time	n_{md}	AR
0.05	2322(130)	50	94%	0.18	1150(40)	30	92%
0.1	1713(200)	30	87%	0.19	1339(80)	30	95%
0.2	1782(130)	30	87%	0.2	1275(70)	30	92%
0.3	1779(110)	30	90%	0.21	2192(100)	30	91%
0.4	1836(180)	30	87%	0.22	2485(130)	30	90%
0.5	1972(220)	30	90%	0.23	1937(190)	30	90%

Table 10

The average timings for one trajectory (in seconds), the number of molecular dynamics steps and the acceptance rate for the $\kappa = 0.225$ ensembles (left), and the $\mu = 0.5$ ensembles (right). The total time of the trajectory, $\Delta\tau n_{md}$, is equal to 1.

5.5 Computer performance

The timings to generate a 4^4 trajectory are shown in table 10. They are based on running on four nodes of the cluster computer ALiCE at Wuppertal University. The 6^4 ensembles (table 11) were generated on eight nodes and the 8^4 ensembles on 16 nodes. [16] We used CG with relaxation and preconditioning [47] to perform the inversion, which has approximately a factor of 4 performance gain over the standard CG. Our timings are quite independent of the mass, although we expect this fact to change on larger and less well conditioned systems. However, the scaling of the computer time with mass will be better than the μ^{-3} behaviour which we assume for Wilson or staggered fermions because with overlap fermions there are fewer crossings for small masses. It can be seen by comparing the timings on the $\mu = 0.5$ ensembles (table 10) below and above the critical κ that at this large mass the time needed for the treatment of the crossings was around 40% of the total computer time (there are usually 3-4 reflection or transmission steps per trajectory at $\mu = 0.5$ and κ well above the critical κ). The acceptance rate was stable for all our 4^4 ensembles. We increased the number of molecular dynamics steps (n_{md}) to 50 (keeping $\Delta\tau\, n_{md} = 1$) for the 4^4 ensemble generated at $\mu = 0.05$ and $\kappa = 0.225$ in order to counteract the large fermionic force in non-trivial topological sectors (see section 5.1), but otherwise we did not have to change the trajectory length as we changed the mass to maintain the acceptance rate. On our larger lattices, we had to increase n_{md} at lower masses.

---

[16] In parallel computations, we estimated—by explicitly calculating the number of floating point operations for one trajectory—that ALiCE runs at around 0.4 GFlops/node for the 4^4 ensembles and 0.7 GFlops/node for the 6^4 and 8^4 ensembles.

Configuration	Time	n_{md}	AR
$6^4 \ \mu = 0.05$	6714(250)	40	84%
$6^4 \ \mu = 0.1$	6674(240)	40	86%
$6^4 \ \mu = 0.3$	5535(110)	30	79%
$8^4 \ \mu = 0.1$	30049(1087)	50	79%
$8^4 \ \mu = 0.3$	26456(540)	40	80%

Table 11

The average timings for one trajectory (in seconds), the number of molecular dynamics steps, and the acceptance rate on the larger lattices, with $\kappa = 0.2$. The total time of the trajectory, is equal to 1 .

6 Conclusions and Outlook

In this paper, we have presented the basics of an improved simulation scheme for full QCD including the chirally symmetric overlap fermion discretization. We have constructed an exact Hybrid Monte Carlo algorithm being capable of generating gauge field configurations with two flavours of dynamical overlap fermions. The HMC algorithm proposed aims at the exploration of the low quark mass regime of lattice QCD with a lattice action observing exact chiral symmetry. The method can be extended to solve the problem of low modes that are mixing as well as to improve topological tunnelling rates.

The main conceptual difficulty constructing a dynamical overlap algorithm is the appearance of a Dirac delta function within the fermionic force. A naive straightforward integration leads to action differences from the discrete leap frog integration which turn out to be much too large to allow acceptance in the global Monte Carlo decision step at the end of a trajectory. These large action differences are caused by zero-mode crossings of the low eigenvalues of the Wilson kernel used within the overlap operator. They force the algorithm to slow down and to get stuck eventually.

In order to avoid the action violations as caused by eigenvalue crossings, we have developed an explicit integration procedure for evolving the low crossing modes within the molecular dynamics part of the HMC. In case of reflection on the action wall the change in energy is zero by definition and also in case of transmission a quite smooth integration over the singularity is achieved. The new scheme can cope with multiple eigenvalue crossings within the same MD time step.

The proposed HMC for overlap fermions has several advantages:

– The action differences are small enough to allow for reasonable acceptance rates of the HMC.

- The scheme is constructed to allow for a systematic improvement of the complexity of the action violation as arising from a finite integration time-step.
- The action violation of the specific realization constructed in this paper is comparable to the $O(\Delta\tau^2)$ error of the standard HMC leap-frog integration over the entire trajectory.
- The algorithm is shown to satisfy reversibility and area conservation.
- The universal ansatz in this paper for the correction step in terms of orthonormal vectors η_k has the potential to construct a *non-area-conserving* higher-order integration method. This approach has the potential to solve the problem of the mixing of low modes that occasionally leads to large action violations on larger lattices, spoiling the acceptance rate even after correction of single mode zero crossings. Such an improved scheme, based on the present approach, will be described in a subsequent paper [55].
- In addition, the universal ansatz of this paper for the correction step is part of the improvement of the tunnelling of the topological index to be described in an upcoming paper [63].

We have tested the algorithm on Teraflop-Class computers with lattice sizes ranging from 4^4 to 8^4, calculating a set of basic physical observables. Despite of large finite-size effects appearing on such small lattices, we do get results for, *e.g.*, the topological susceptibility, which behave qualitatively as expected. This demonstrates that intermediate lattices are in reach of Teraflop-class computers.

With the help of the new algorithm and improvements to be presented in three forthcoming papers [55,63,64], larger lattice sizes, required to realize physically meaningful systems, will become accessible on upcoming Petaflop-class systems.

Acknowledgements

Appendix

A   Detailed Balance and the Size of the Correction Step Error

In this section we prove that the general correction update (46) satisfies detailed balance. Extending this proof to the slightly modified update in equations (50) and (51) is straightforward.

A.1   Detailed balance and reversibility

The initial and final leap frog steps (steps 1 and 2, and 6 and 7) in algorithm 2 are known to be reversible. Thus, it just has to be shown that the correction steps (steps 3, 4 and 5) are reversible. Here, the proof of reversibility for the correction step for the case of transmission in algorithm 2 is given. The proof for the reflection update is similar.

A.1.1   The momentum update

It is assumed that when reversing the sign of $\Delta\tau$, $d_k \to -d_k$ $\forall k$. This condition is satisfied for our algorithms, because τ_c and η_k^j remain constant, $F^+ \to F^-$ and $d \to -d$, since the sign of the smallest eigenvalue is opposite for the

39

reverse update. Our general transmission momentum update (46) reads:

$$
\begin{aligned}
\Pi^+ =& \Pi^- - \tau_c(F^- - F^+) + \tau_c\eta(\eta, F^- - F^+) + \frac{1}{3}\mathrm{Tr}(F^- - F^+) + \\
& \eta(\Pi^-, \eta)\left(\sqrt{1 + \frac{d_1}{(\Pi^-, \eta)^2}} - 1\right) \\
& + \sum_k \left(\eta_1^k(\eta_1^k, \Pi^- - \frac{\tau_c}{2}(F^- + F^+)) + \eta_1^k(\eta_2^k, \Pi^- - \frac{\tau_c}{2}(F^- + F^+))\right) \times \\
& \left(\sqrt{1 + \frac{d_k}{(\eta_1^k, \Pi^- - \frac{\tau_c}{2}(F^- + F^+))^2 + (\eta_2^k, \Pi^- - \frac{\tau_c}{2}(F^- + F^+))^2}} - 1\right),
\end{aligned}
\tag{A.1}
$$

so that

$$
\begin{aligned}
(\Pi^+, \eta) =& (\Pi^-, \eta)\sqrt{1 + \frac{d_1}{(\Pi^-, \eta)^2}}; \\
(\Pi^+ + \frac{\tau_c}{2}(F^- + F^+), \eta_{k_i}) =& (\eta_{k_i}, \Pi^- - \frac{\tau_c}{2}(F^- + F^+)) \times \\
& \left(\sqrt{1 + \frac{d_k}{(\eta_1^k, \Pi^- - \frac{\tau_c}{2}(F^- + F^+))^2 + (\eta_2^k, \Pi^- - \frac{\tau_c}{2}(F^- + F^+))^2}} - 1\right).
\end{aligned}
\tag{A.2}
$$

The time-reverse update, with $\Delta\tau \to -\Delta\tau$, is given by

$$
\begin{aligned}
\Pi'_- =& \Pi^+ + \tau_c(F^+ - F^-) - \tau_c\eta(\eta, F^+ - F^-) - \frac{1}{3}\mathrm{Tr}(F^- - F^+) + \\
& \eta(\Pi^+, \eta)\left(\sqrt{1 - \frac{d_1}{(\Pi^+, \eta)^2}} - 1\right) + \\
& \sum_k \left(\eta_1^k(\eta_1^k, \Pi^+ - \frac{\tau_c}{2}(F^- + F^+)) + \eta_2^k(\eta_2^k, \Pi^+ - \frac{\tau_c}{2}(F^- + F^+))\right) \times \\
& \left(\sqrt{1 - \frac{d_k}{(\eta_1^k, \Pi^+ - \frac{\tau_c}{2}(F^- + F^+))^2 + (\eta_2^k, \Pi^+ - \frac{\tau_c}{2}(F^- + F^+))^2}} - 1\right).
\end{aligned}
\tag{A.3}
$$

40

We note that

$$(\Pi^+, \eta) \left(\sqrt{1 - \frac{d_1}{(\Pi^+, \eta)^2}} - 1 \right)$$

$$= (\Pi^-, \eta) \sqrt{1 + \frac{d_1}{(\Pi^-, \eta)^2}} \left(\sqrt{1 - \frac{d_1}{(\Pi^-, \eta)^2 \left(1 + \frac{d_1}{(\Pi^-, \eta)^2}\right)}} - 1 \right)$$

$$= (\Pi^-, \eta) \left(1 - \sqrt{1 + \frac{d_1}{(\Pi^-, \eta)^2}} \right); \tag{A.4}$$

$$(\Pi^+ - \frac{\tau_c}{2}(F^- + F^+), \eta_1^k) \times$$

$$\left(\sqrt{1 - \frac{d_k}{(\eta_1^k, \Pi^+ + \frac{\tau_c}{2}(F^- + F^+))^2 + (\eta_2^k, \Pi^+ - \frac{\tau_c}{2}(F^- + F^+))^2}} - 1 \right)$$

$$= - (\Pi^- - \frac{\tau_c}{2}(F^- + F^+), \eta_1^k) \times$$

$$\left(\sqrt{1 + \frac{d_k}{(\eta_1^k, \Pi^- - \frac{\tau_c}{2}(F^- + F^+))^2 + (\eta_2^k, \Pi^- - \frac{\tau_c}{2}(F^- + F^+))^2}} - 1 \right). \tag{A.5}$$

Combining (A.1), (A.3), (A.4) and (A.5) gives $\Pi'_- = \Pi^-$; therefore, the momentum update is reversible.

A.1.2 The gauge field update

The gauge field update is given by:

$$U^+ = e^{-i\tau_c \Pi^+} e^{i\tau_c \Pi^-} U^-. \tag{A.6}$$

Switching $\Delta\tau \to -\Delta\tau$ leads to

$$U'_- = e^{-i\tau_c \Pi^-} e^{i\tau_c \Pi^+} U^+, \tag{A.7}$$

which gives $U'_- = U^-$; therefore, the gauge field update is reversible.

A.2 Detailed Balance: Area Conservation

A.2.1 Transmission

The transmission update, given by algorithm 2 and using equation (46) can be shown to be area conserving. For simplicity, it is assumed that d_1 is a function of the gauge field at the crossing only and has no additional dependence on

Π, and all the other d_ks are functions of the gauge field of the crossing and (η, Π) only. The matrices η_j^i and the fermionic forces $F^\pm$ are just functions of the gauge field at the crossing. These conditions can be relaxed, but not necessarily for the purpose of this paper.

D_i is a derivative of the gauge fields U, defined as

$$D_i f(U) = \lim_{h \to 0} \frac{\partial}{\partial h} f\left(e^{ihT_i}U\right), \tag{A.8}$$

where T_i are some suitable generators of the $SU(N_C)$ gauge group (*e.g.* in SU(3), $T_i = \lambda_i/2$, where λ_i are the Gell-Mann matrices). One can write the gauge fields in terms of $N_C^2 - 1$ parameters r_i so that

$$D_i f(U) = \frac{\partial}{\partial r_i} f(U). \tag{A.9}$$

Similarly, one can define coordinates for the momentum Π and the matrix η in terms of the generators T:

$$\Pi_\mu(x) = \pi_i^{x\mu} T_i, \qquad \eta_\mu(x) = \eta_i^{x\mu} T_i, \qquad F_\pm - \frac{1}{3}\text{Tr}(F_\pm) = f_{\pm i}^{x\mu} T_i,$$
$$\eta_{j,\mu}^k(x) = n_{j,i}^{k,x\mu} T_i. \tag{A.10}$$

x refers to the lattice site, and μ is a direction index. The normalization condition $(\eta, \eta) = 1$ implies that n_j^k is normalized according to $n_{j,i}^{k,x\mu} n_{j,i}^{k,x\mu} = 2$. For notational convenience, we shall define:

$$N_i^{x\mu}(U, \Pi) = \frac{1}{2}\eta_i^{x\mu}(U)\eta_j^{y\nu}(U)\pi_j^{y\nu}\left(\sqrt{1 + \frac{4d_1}{(\eta_k^{z\rho}(U)\pi_k^{z\rho})^2}} - 1\right) -$$
$$\tau_c\left(\delta_{ij}\delta^{xy}\delta^{\mu\nu} - \eta_i^{x\mu}(U)\eta_j^{y\nu}(U)\right)\left(f_{-j}^{y\nu}(U) - f_{+j}^{y\nu}(U)\right) +$$
$$\sum_k\left(n_{1,i}^{k,x\mu}(U)N_{e1}^k(U, \Pi) + n_{2,i}^{k,x\mu}(U)N_{e2}^k(U, \Pi)\right)$$
$$\left(\sqrt{1 + \frac{d_k}{(N_{e1}^k(U, \Pi))^2 + (N_{e2}^k(U, \Pi))^2}} - 1\right). \tag{A.11}$$
$$N_{e1}^k = \frac{1}{2}\left(n_{1,j}^{k,z\rho}\left(\pi_j^{z\rho} - \frac{\tau_c}{2}(f_{+j}^{z\rho} - f_{-j}^{z\rho})\right)\right),$$
$$N_{e2}^k = \frac{1}{2}\left(n_{2,j}^{k,z\rho}\left(\pi_j^{z\rho} - \frac{\tau_c}{2}(f_{+j}^{z\rho} - f_{-j}^{z\rho})\right)\right). \tag{A.12}$$

The generator of a time update $\Delta\tau$ is

$$e^{\Delta\tau\frac{\partial}{\partial\tau}} = e^{\Delta\tau\left(\frac{\partial\pi_i}{\partial\tau}\frac{\partial}{\partial\pi_i} + \frac{\partial r_i}{\partial\tau}\frac{\partial}{\partial r_i}\right)}$$
$$= e^{\Delta\tau\left(-\frac{\partial E}{\partial r_i}\frac{\partial}{\partial\pi_i} + \frac{\partial E}{\partial\pi_i}\frac{\partial}{\partial r_i}\right)}$$
$$= e^{\Delta\tau\hat{H}}. \tag{A.13}$$

For the standard leapfrog update, we define the operators

$$\hat{P} = e^{\frac{\Delta\tau}{2}F'_i\frac{\partial}{\partial\pi_i}}$$
$$\hat{Q} = e^{\frac{\Delta\tau}{2}\pi_i\frac{\partial}{\partial r_i}}, \tag{A.14}$$

then we have

$$\hat{P}f(\pi,r) = f(\pi + F'\frac{\Delta\tau}{2}, r) \qquad \hat{Q}f(\pi,r) = f(\pi, r + \frac{\Delta\tau}{2}\pi). \tag{A.15}$$

F' is the total force in the momentum update (the sum of the gauge field and fermionic forces). The standard leapfrog update is given by

$$\hat{P}\hat{Q}\hat{Q}\hat{P} = e^{\Delta\tau(\hat{H}+O(\Delta\tau^2))}. \tag{A.16}$$

$\hat{P}\hat{Q}\hat{Q}\hat{P}$ is manifestly area conserving, because the operators $\hat{P}$ and $\hat{Q}$ are area conserving.

For the correction step, we need to define two new update operators, $\hat{P}_c$ and $\hat{Q}_c$, so that $\hat{Q}_c f(\pi,r) = f(\pi, r - \tau_c\pi)$ and $\hat{P}_c f(\pi,r) = f(\pi + N_i, r)$. $\hat{P}_c$ and $\hat{Q}_c$ are

$$\hat{P}_c = 1 + N_i\frac{\partial}{\partial\pi_i} + \frac{1}{2}N_iN_j\frac{\partial^2}{\partial\pi_i\pi_j} + \frac{1}{6}N_iN_jN_k\frac{\partial^3}{\partial\pi_i\pi_j\pi_k} + \dots$$
$$\hat{Q}_c = 1 - \tau_c\pi_i\frac{\partial}{\partial r_i} + \frac{1}{2}\tau_c^2\pi_i\pi_j\frac{\partial^2}{\partial r_ir_j} + \frac{1}{6}\tau_c^3\pi_i\pi_j\pi_k\frac{\partial^3}{\partial r_ir_jr_k} + \dots. \tag{A.17}$$

Because $[\partial/\partial r_i, \tau_c] \neq 0$ and $[\partial/\partial r_i, N_j] \neq 0$, we cannot factorise $\hat{P}_c$ and $\hat{Q}_c$ into a simple exponential form, although using equation (A.9) we can write

$$\hat{Q}_c U = e^{-i\tau_c\pi_i T_i}U = e^{-i\tau_c\Pi^-}U. \tag{A.18}$$

These operators by themselves are not area conserving. The full correction update is $\hat{Q}_c^\dagger\hat{P}_c\hat{Q}_c$:

$$\hat{Q}_c^\dagger\hat{P}_c\hat{Q}_c\Pi^- = \Pi^- + \frac{1}{2}\eta(\eta_j^{x\mu}\pi_j^{x\mu})\left(\sqrt{1 + \frac{4d_1}{(\eta_m^{y\nu}(\tau_c)\pi_m^{y\nu})^2}} - 1\right) +$$
$$(F^+ - F^-) - \frac{1}{2}\eta\eta_j^{x\mu}(f_+ - f_-)_j^{x\mu} +$$
$$\sum_k(\eta_1^kN_{e1}^k + \eta_2^kN_{e2}^k)\left(\sqrt{1 + \frac{d_k}{(N_{e1}^k)^2 + (N_{e2}^k)^2}} - 1\right) = \Pi^+$$
$$\hat{Q}_c^\dagger\hat{P}_c\hat{Q}_c U^- = \hat{Q}_c^\dagger\hat{P}_c e^{-i\tau_c\Pi^-}U^-$$
$$= \hat{Q}_c^\dagger e^{-i\tau_c(\Pi^- + N(U^-,\Pi^-))}U^-$$
$$= e^{-i\tau_c(\Pi_- + N(U_c,\Pi_-))}e^{i\tau_c\Pi^-}U^- = U^+, \tag{A.19}$$

where d, f, η etc. are all calculated at the crossing gauge field U_c. Therefore, the update in algorithm 2 can be written as $\hat{P}\hat{Q}\hat{Q}_c^{\dagger}\hat{P}_c\hat{Q}_cQP$. We know that $\hat{P}$ and $\hat{Q}$ are area conserving, so we just need to show that $\hat{Q}_c^{\dagger}\hat{P}_c\hat{Q}_c$ is also area conserving. We write the updated gauge field and momentum as q and p respectively (recalling that the initial fields were r and π in our notation). This gives us

$$
\begin{aligned}
p_i^{x\mu} = \hat{Q}_c^{\dagger}\hat{P}_c\hat{Q}_c\pi_i^{x\mu} &= \pi_i^{x\mu} + \frac{1}{2}\eta_i^{x\mu}\pi_j^{y\nu}\eta_j^{y\nu}\left(\sqrt{1+\frac{4d_1}{(\pi_m^{z\rho}\eta_m^{z\rho})^2}}-1\right) - \\
&\tau_c\left(\delta_{ij}\delta^{xy}\delta^{\mu\nu}-\frac{1}{2}\eta_i^{x\mu}\eta_j^{y\nu}\right)\left(f_{-j}^{y\nu}-f_{+j}^{y\nu}\right) + \\
&\sum_k\left(n_{1,i}^{k,x\mu}N_{e1}^k+n_{2,i}^{k,x\mu}N_{e2}^k\right)\left(\sqrt{1+\frac{d_k}{(N_{e1}^k)^2+(N_{e2}^k)^2}}-1\right);
\end{aligned}
$$

(A.20)

$$
q_i^{x\mu} = \hat{Q}_c^{\dagger}\hat{P}_c\hat{Q}_c r = r_i^{x\mu} + \tau_c(\pi_i^{x\mu}-p_i^{x\mu}).
$$

(A.21)

It has to be shown that the determinant

$$
J = \begin{vmatrix} \frac{\partial p_i}{\partial \pi_m} & \frac{\partial q_i}{\partial \pi_m} \\ \frac{\partial p_i}{\partial r_m} & \frac{\partial q_i}{\partial r_m} \end{vmatrix} = 1.
$$

(A.22)

r_c is the gauge field at the eigenvalue crossing:

$$
r_{ci}^{x\mu} = \hat{Q}_c r_i^{x\mu} = r_i^{x\mu} + \pi_i^{x\mu}\tau_c.
$$

(A.23)

Thus, we can write

$$
\tau_c = \frac{(r_c^{y\nu}-r^{y\nu})_i\eta_i^{y\nu}}{\pi_j^{z\rho}\eta_j^{z\rho}},
$$

(A.24)

$$
\frac{\partial\tau_c}{\partial\pi_k^{x\mu}} = \frac{1}{\pi_j^{z\rho}\eta_j^{z\rho}}\left(\frac{\partial r_{ci}^{y\nu}}{\partial\pi_k^{x\mu}}\eta_i^{y\nu}-\tau_c\eta_k^{x\mu}+\frac{\partial\eta_j^{y\nu}}{\partial\pi_k^{x\mu}}\left(r_c^{y\nu}-r^{y\nu}-\tau_c\pi^{y\nu}\right)_j\right),
$$

(A.25)

$$
\frac{\partial\tau_c}{\partial r_k^{x\mu}} = \frac{1}{\pi_j^{z\rho}\eta_j^{z\rho}}\left(\frac{\partial r_{ci}^{y\nu}}{\partial r_k^{x\mu}}\eta_i^{y\nu}-\eta_k^{x\mu}+\frac{\partial\eta_j^{y\nu}}{\partial r_k^{x\mu}}\left(r_c^{y\nu}-r^{y\nu}-\tau_c\pi^{y\nu}\right)_j\right).
$$

(A.26)

We choose η so that

$$
\frac{\partial r_{ci}^{y\nu}}{\partial r_k^{x\mu}}\eta_i^{y\nu} = \frac{\partial r_{ci}^{y\nu}}{\partial\pi_k^{x\mu}}\eta_i^{y\nu} = 0.
$$

(A.27)

Hence

$$
\frac{\partial\tau_c}{\partial\pi_k^{x\mu}} = \tau_c\frac{\partial\tau_c}{\partial r_k^{x\mu}} = -\tau_c\frac{\eta_k^{x\mu}}{\pi_j^{z\rho}\eta_j^{z\rho}}.
$$

(A.28)

Since r_c is a point on the surface of constant $\lambda = 0$, one solution to (A.27) is

that η_i is normal to this surface, i.e. proportional to the vector

$$\frac{\partial \lambda}{\partial r_{ci}^{x\mu}} = -\kappa \langle \psi(x)|\gamma_5 \left((1-\gamma_\mu)\frac{\partial U}{\partial r_{ci}^{x\mu}}\delta_{x,y+\mu} + (1+\gamma_\mu)\frac{\partial U^\dagger}{\partial r_{ci}^{x\mu}}\delta_{x,y-\mu} \right)|\psi(y)\rangle.$$
(A.29)

We also have for any function g of $r + \pi\tau_c$ (such as η or d),

$$\frac{\partial g}{\partial \pi_k^{z\rho}} = \tau_c \frac{\partial g}{\partial r_k^{z\rho}}.$$
(A.30)

We are now in a position to write down the components of J by differentiating (A.20) and (A.21). By writing p and q as functions of r_c and π, we have

$$\left(\frac{\partial p_i^{x\mu}}{\partial \pi_m^{y\nu}}\right)_r = \left(\frac{\partial p_i^{x\mu}}{\partial \pi_m^{y\nu}}\right)_{r_c} + \left(\frac{\partial p_i^{x\mu}}{\partial r_{cj}^{z\rho}}\right)_\pi \left(\frac{\partial r_{cj}^{z\rho}}{\partial \pi_m^{y\nu}}\right)_r$$

$$= \left(\frac{\partial p_i^{x\mu}}{\partial \pi_m^{y\nu}}\right)_{r_c} + \tau_c \left(\frac{\partial p_i^{x\mu}}{\partial r_m^{y\nu}}\right)_\pi$$

$$= \delta_{im}\delta_{xy}\delta_{\mu\nu} + \frac{1}{2}\eta_i^{x\mu}\eta_m^{y\nu}\left(\frac{1}{\sqrt{1+\frac{4d_1}{(\pi_n^{z\rho}\eta_n^{z\rho})^2}}} - 1\right) + \tau_c\frac{\partial p_i^{x\mu}}{\partial r_m^{y\nu}} +$$

$$\frac{1}{2}\sum_k n_{1,i}^{k,x\mu}n_{1,m}^{k,y\nu}\left(-1+\frac{1+(N_{e2}^k)^2\frac{d_k}{((N_{e1}^k)^2+(N_{e2}^k)^2)^2}}{\sqrt{1+\frac{d_k}{(N_{e1}^k)^2+(N_{e2}^k)^2}}}\right) +$$

$$\frac{1}{2}\sum_k n_{2,i}^{k,x\mu}n_{2,m}^{k,y\nu}\left(-1+\frac{1+(N_{e1}^k)^2\frac{d_k}{((N_{e1}^k)^2+(N_{e2}^k)^2)^2}}{\sqrt{1+\frac{d_k}{(N_{e1}^k)^2+(N_{e2}^k)^2}}}\right) -$$

$$\frac{1}{2}\sum_k \left(n_{1,i}^{k,x\mu}n_{2,m}^{k,y\nu} + n_{2,i}^{k,x\mu}n_{1,m}^{k,y\nu}\right)\left(\frac{N_{e1}^k N_{e2}^k \frac{d_k}{((N_{e1}^k)^2+(N_{e2}^k)^2)^2}}{\sqrt{1+\frac{d_k}{(N_{e1}^k)^2+(N_{e2}^k)^2}}}\right) +$$

$$\frac{1}{2}\sum_k \left(n_{1,i}^{k,x\mu}N_{e1}^k + n_{2,i}^{k,x\mu}N_{e2}^k\right)\eta_m^{k,y\nu}\frac{\left(\frac{\partial d_k}{\partial(\eta_n^{z\rho}\pi_n^{z\rho})}\right)_{r_c}}{\sqrt{1+\frac{d_k}{(N_{e1}^k)^2+(N_{e2}^k)^2}}}.$$
(A.31)

$$\frac{\partial q_i^{x\mu}}{\partial \pi_m^{y\nu}} = -\tau_c\frac{\partial p_i^{x\mu}}{\partial \pi_m^{y\nu}} + \tau_c\left(\frac{\partial q_i^{x\mu}}{\partial r_m^{y\nu}} + \tau_c\frac{\partial p_i^{x\mu}}{\partial r_m^{y\nu}}\right).$$
(A.32)

$$\frac{\partial q_i^{x\mu}}{\partial r_m^{y\nu}} = \delta_{im}\delta_{xy}\delta_{\mu\nu} - \frac{\eta_m^{y\nu}}{\eta_j^{z\rho}\pi^{z\rho_j}}(\pi_i^{x\mu} - p_i^{x\mu}) - \tau_c\frac{\partial p_i^{x\mu}}{\partial r_m^{y\nu}}.$$
(A.33)

45

Therefore, the Jacobian is

$$
\begin{aligned}
J &= \begin{vmatrix} \frac{\partial p_i}{\partial \pi_k} & \frac{\partial q_i}{\partial \pi_k} \\[2mm] \frac{\partial p_i}{\partial r_k} & \frac{\partial q_i}{\partial r_k} \end{vmatrix} = \begin{vmatrix} \frac{\partial p_i}{\partial \pi_i} & \frac{\partial q_i}{\partial \pi_k} + \tau_c \frac{\partial p_i}{\partial \pi_k} \\[2mm] \frac{\partial p_i}{\partial r_k} & \frac{\partial q_i}{\partial r_k} + \tau_c \frac{\partial p_i}{\partial r_k} \end{vmatrix} \\[4mm]
&= \begin{vmatrix} \frac{\partial p_i}{\partial \pi_k} - \tau_c \frac{\partial p_i}{\partial r_k} & \frac{\partial q_i}{\partial \pi_k} + \tau_c \frac{\partial p_i}{\partial \pi_k} - \tau_c \left(\frac{\partial q_i}{\partial r_k} + \tau_c \frac{\partial p_i}{\partial r_k} \right) = 0 \\[2mm] \frac{\partial p_i}{\partial r_k} & \frac{\partial q_i}{\partial r_k} + \tau_c \frac{\partial p_i}{\partial r_k} \end{vmatrix} .
\end{aligned}
\tag{A.34}
$$

So J is the product of the two determinants

$$
\left| \frac{\partial p_i}{\partial \pi_m} - \tau_c \frac{\partial p_i}{\partial r_m} \right| = \frac{1}{\sqrt{1 + \frac{4d_1}{(\pi_n^{z\rho} \eta_n^{z\rho})^2}}},
\tag{A.35}
$$

and

$$
\left| \frac{\partial q_i}{\partial r_m} + \tau_c \frac{\partial p_i}{\partial r_m} \right| = \sqrt{1 + \frac{4d_1}{(\pi_n^{z\rho} \eta_n^{z\rho})^2}}.
\tag{A.36}
$$

The two determinants (equations (A.35) and (A.36)) can easily be calculated by using the relations $|\delta_{ij} + N_i^a M_{ab} N_j^b| = |\delta_{ab} + M_{ab}|$ (where $N_i^a N_i^b = \delta_{ab}$ and N_i^a are real) and $|\delta_{ij} + v_i u_j| = 1 + v_i u_i$, and by recalling that $\eta_i^{x\mu}$ and $n_{1,i}^{k,x\mu}$ are normalised to 2. Note that equation (A.36) would not hold if we included terms in the fermionic force parallel to η. Multiplying the two determinants together gives $J = 1$. Therefore, this procedure is area conserving.

A.2.2 Reflection

The proof that the reflection algorithm is area conserving follows the same line as that for transmission: instead of equations (A.35) and (A.36), we get

$$
\left| \frac{\partial p_i}{\partial \pi_m} - \tau_c \frac{\partial p_i}{\partial r_m} \right| = -1
\tag{A.37}
$$

$$
\left| \frac{\partial q_i}{\partial r_m} + \tau_c \frac{\partial p_i}{\partial r_m} \right| = 1,
\tag{A.38}
$$

which gives $J = -1$.

A.2.3 The combined update step

There is one further requirement for area conservation to be satisfied. It is not sufficient for the standard update and the corrected update to be area conserving separately; the combination of them which we use in our molecular

dynamics procedure must also conserve the measure. We define $F_T^{\Pi,U}$ and $F_R^{\Pi,U}$ as the momentum updates for transmission and reflection respectively. We write the transmission condition as $x(\Pi^-, U_C) > 0$, so we transmit when this condition holds and reflect when $x < 0$. The question remains what we should do at $x = 0$, and that is what we shall address in this section. x is a function of the initial momentum and the gauge field at the crossing (which is itself a function of the initial momentum and the initial gauge field, as discussed above). We can therefore write the momentum and gauge updates combining the reflection and transmission updates as

$$p_i = F_{Ti}^{\Pi}\theta\left(x\right) + \left(1 - \theta\left(x\right)\right)F_{Ri}^{\Pi}, \tag{A.39}$$

$$q_i = F_{Ti}^{U}\theta\left(x\right) + \left(1 - \theta\left(x\right)\right)F_{Ri}^{U}. \tag{A.40}$$

$\theta(x)$ is the step function, i.e. $\theta = 1$ for $x > 0$ and $\theta(x) = 0$ for $x < 0$. We can now differentiate these equations to get the Jacobian (using the same determinant manipulation as before in an attempt to bring one of the sub-determinants to zero):

$$J = \begin{vmatrix} \frac{\partial p_i}{\partial \pi_j} & \frac{\partial q_i}{\partial \pi_j}; \\ \frac{\partial p_i}{\partial r_j} & \frac{\partial q_i}{\partial r_j} \end{vmatrix} = \begin{vmatrix} J_{11} & J_{12} \\ J_{21} & J_{22} \end{vmatrix} \tag{A.41}$$

$$J_{11} = \theta(x)\left(\frac{\partial F_{Ti}^{\Pi}}{\partial \pi_j} - \tau_c\frac{\partial F_{Ti}^{\Pi}}{\partial r_j}\right) + \left(1 - \theta(x)\right)\left(\frac{\partial F_{Ri}^{\Pi}}{\partial \pi_j} - \tau_c\frac{\partial F_{Ri}^{\Pi}}{\partial r_j}\right) +$$
$$\delta(x)\left(\frac{\partial x}{\partial \pi_j} + \frac{\partial x}{\partial r_c}\frac{\partial r_c}{\partial \pi_j} - \tau_c\frac{\partial x}{\partial r_c}\frac{\partial r_c}{\partial r_j}\right)\left(F_{Ti}^{\Pi} - F_{Ri}^{\Pi}\right) \tag{A.42}$$

$$J_{12} = \theta(x)\left(\frac{\partial F_{Ti}^{U}}{\partial \pi_j} - \tau_c\frac{\partial F_{Ti}^{U}}{\partial r_j} + \tau_c\frac{\partial F_{Ti}^{\Pi}}{\partial \pi_j} - \tau_c^2\frac{\partial F_{Ti}^{\Pi}}{\partial r_j}\right) +$$
$$\left(1 - \theta(x)\right)\left(\frac{\partial F_{Ri}^{U}}{\partial \pi_j} - \tau_c\frac{\partial F_{Ri}^{U}}{\partial r_j} - \tau_c\frac{\partial F_{Ri}^{\Pi}}{\partial \pi_j} + \tau_c^2\frac{\partial F_{Ri}^{\Pi}}{\partial r_j}\right) +$$
$$\theta(x)\left(1 - \theta(x)\right)\left(-\tau_c\frac{\partial F_{Ti}^{U}}{\partial r_j} + \tau_c^2\frac{\partial F_{Ti}^{\Pi}}{\partial r_j} + \tau_c\frac{\partial F_{Ri}^{U}}{\partial r_j} - \tau_c^2\frac{\partial F_{Ri}^{\Pi}}{\partial r_j}\right) +$$
$$\delta(x)(F_{Ti}^{U} - F_{Ri}^{U})\left(\frac{\partial x}{\partial r_c}\frac{\partial r_c}{\partial \pi_j} - \frac{\partial x}{\partial r_c}\frac{\partial r_c}{\partial r_j}\tau_c + \frac{\partial x}{\partial \pi_j}\right) +$$
$$\delta(x)\tau_c(F_{Ti}^{\Pi} - F_{Ri}^{\Pi})(2\theta(x) - 1)\left(\frac{\partial x}{\partial r_c}\frac{\partial r_c}{\partial \pi_j} - \frac{\partial x}{\partial r_c}\frac{\partial r_c}{\partial r_j}\tau_c + \frac{\partial x}{\partial \pi_j}\right); \tag{A.43}$$

$$J_{21} = \theta(x)\frac{\partial F_{Ti}^{\Pi}}{\partial r_j} + \left(1 - \theta(x)\right)\frac{\partial F_{Ri}^{\Pi}}{\partial r_j} + \delta(x)\left(F_{Ti}^{\Pi} - F_{Ri}^{\Pi}\right)\frac{\partial x}{\partial r_c}\frac{\partial r_c}{\partial r_j}; \tag{A.44}$$

47

$$J_{22} = \theta(x) \left(\frac{\partial F_{Ti}^U}{\partial r_j} + \tau_c \frac{\partial F_{Ti}^\Pi}{\partial r_j} \right) + (1 - \theta(x)) \left(\frac{\partial F_{Ti}^U}{\partial r_j} - \tau_c \frac{\partial F_{Ti}^\Pi}{\partial r_j} \right) +$$

$$\theta(x)(1 - \theta(x))\tau_c \left(-\frac{\partial F_{Ti}^\Pi}{\partial r_j} + \frac{\partial F_{Ri}^\Pi}{\partial r_j} \right) +$$

$$\delta(x)\frac{\partial x}{\partial r_c} \left(\frac{\partial r_c}{\partial r_j}(F_{Ti}^U - F_{Ri}^U) + \tau_c(2\theta(x) - 1)\left(\frac{\partial r_c}{\partial r_j}(F_{Ti}^\Pi - F_{Ri}^\Pi) \right) \right). \quad \text{(A.45)}$$

The $[2\theta(x) - 1]$-terms are caused by the different updates of the gauge field in the algorithms for reflection and transmission. In one case, we need to add the first column to the second column in the determinant calculation; in the other case we need to subtract. These terms, when they are multiplied by the step functions in p and q, additionally lead to the factors of $[\theta(x)(1 - \theta(x))]$. $[\theta(x)(1 - \theta(x))]$-terms will not contribute to the Jacobian unless multiplied by a δ-function (even though they will in practice be multiplied by factors containing $1/\sqrt{x}$): they are finite at $x = 0$ and zero everywhere else: they will not contribute to an integral (we define $\mathbb{D}(x)$ as a function which is 1 at $x = 0$ and zero elsewhere. This can be seen simply by noting that the integration over these terms (either in terms of the gauge fields or the momentum) is zero. Alternatively, this can be shown by an explicit calculation using a particular momentum update. For example, using the algorithm presented in [26], which has $d_1 = 4d$ and $x = 1 + 4d/(\eta, \Pi^-)^2$ (and a slightly different reflection routine) one can demonstrate that the total Jacobian, including these terms, is

$$J = 1 + (1 - x)^2 \frac{d}{dx} \left(\frac{2\theta(x) - (1 + \sqrt{x})\theta^2(x)}{\sqrt{x} - 1} \right) = 1 - 2\delta(x). \quad \text{(A.46)}$$

The rest of the determinant can be simplified by using the results of the previous two sections, particularly the result $\tau_c \partial r_c / \partial r_i = \partial r_c / \partial x_i$. The non-$\delta$-function terms in J_{12} cancel immediately as before. Because the terms multiplying the δ-functions are the outer product of two matrices, we can remove all but one of these functions by determinant manipulation. For example, by subtracting $\partial x / \partial \pi_j \mathbb{D}(x)/(\partial x / \partial r_c \partial r_c / \partial r$ multiplied by J_{11} and J_{12} from the J_{21} and J_{22} allows us to remove the δ-functions in those terms, and a similar manipulation allows the removal of the δ-function in J_{12}, so that the only δ-function which remains is contained within J_{11}. We can use a Schur decomposition to factorise the determinant in a similar manner to before

$$J = \left| J_{11} - J_{12} J_{22}^{-1} J_{21} \right| |J_{22}|. \quad \text{(A.47)}$$

$|J_{22}|$ contains no δ-function. Because the Schur compliment is proportional to $\mathbb{D}$ and contains no δ-functions, it will not contribute when we integrate over it. But the single δ-function, multiplied by $\partial x / \partial \pi_j$, in J_{11} remains. We can use a stopping criterion with $\partial x / \partial \pi_j \ll 1$ (setting $\partial x / \partial \pi_j = 0$ renders the above argument invalid, but we can safely set it arbitrarily close to zero then take a

limit) will remove the effect of the δ-function in a numerical simulation; and we use this result to justify our numerical tests in section 5.4. But in a real life simulation we cannot use a fixed x, and we have to determine whether the δ-function in the Jacobian will affect the final results. Except at precisely $x = 0$, the Jacobian is 1.

A.2.4 Discussion of impact of the δ-function Jacobian

We now turn our attention to the question of whether the δ-function of equation (A.47) will affect the equilibrium ensemble of the Monte Carlo.

The updating procedure needs to satisfy

$$W_c[U'] = \int d[U]P[U' \leftarrow U]W_c[U], \tag{A.48}$$

where the probability of moving from a gauge field U to the gauge field U' is $P[U' \leftarrow U]$, and W_c is the canonical distribution for the gauge fields. This is satisfied by the detailed balance condition

$$\int d[\Phi]d[\Phi^\dagger]P[U' \leftarrow U, \Phi]W_c[U, \Phi] = \int d[\Phi]d[\Phi^\dagger]P[U \leftarrow U', \Phi]W_c[U', \Phi]. \tag{A.49}$$

To prove the detailed balance condition for the HMC [81], we define

$$\begin{aligned}
P_\Pi[\Pi] &= e^{-\frac{1}{2}\Pi^2} \\
W_c[U, \Phi] &= e^{-\Phi^\dagger \frac{1}{H^2[U]}\Phi}e^{-S_g[U]} \\
P_A([\Pi', \Phi, U'] \leftarrow [\Pi, \Phi, U]) &= \min\left(1, e^{-E[\Pi', \Phi, U'] + E[\Pi, \Phi, U]}\right) \\
P_\Pi W_c[U] &= e^{-E([\Pi, \Phi, U])} \\
P_{MD}([\Pi', \Phi, U'] \leftarrow [\Pi, \Phi, U]) &= \delta([\Pi', \Phi, U'] - T_{MD}[\Pi, \Phi, U]),
\end{aligned} \tag{A.50}$$

where T_{MD} is the molecular dynamics trajectory, and

$$\begin{aligned}
P[U' \leftarrow U, \Phi] = \int d[\Pi]d[\Pi']P_\Pi[\Pi] \\
P_A([\Pi', \Phi, U'] \leftarrow [\Pi, \Phi, U])P_{MD}([\Pi', \Phi, U'] \leftarrow [\Pi, \phi, U]).
\end{aligned} \tag{A.51}$$

If the Jacobian (which is introduced when the variables are changed in the P_{MD} term) is of the form $J = 1 + J(\Pi)\delta(\Pi - \Pi_c)$, then when we perform the integration over momentum, the detailed balance condition given in equation (A.49) will pick up an additional term when integrating over momentum fields.

It is tempting to argue that because the condition $x = 0$ will never be encountered in a numerical simulation we can neglect this Jacobian while implementing the algorithm; we can, for example, place the logarithm of the Jacobian in

the Metropolis step, and say that we will account for it precisely when $x = 0$, which will never happen in a numerical simulation. However, arguments based around saying that the condition will never be encountered are in effect saying that the measure (in terms of the integration over the initial momentum field) is zero; which is not enough to counter the effect of a Dirac δ-function. Therefore another argument is needed to demonstrate that this will not contribute to the final ensemble. One can also argue the Jacobian will not contribute because we can use an approximate overlap operator, which we will gradually transform to the sign function. The algorithm with the approximate overlap operator will resemble the transmission/reflection algorithm, and it is clearly correct. However, this argument fails because as the approximation of the sign function improves so the molecular dynamics time step must decrease to correctly resolve the step. We, however, are working at a far larger time step than which is necessary to resolve the sign function: the two cases are different. If algorithm works at infinitesimal time-step it does not necessarily follow that it is valid at a finite time step. Therefore, we must find another way of proving that this δ-function does not contribute, or, if it does contribute, how we can compensate for it.

We proceed by explicitly performing the momentum integral in the detailed balance equation over the Dirac δ-functions from the Jacobian; and we shall show that the contribution from the δ-functions cancel out, meaning that detailed balance is maintained. This can be done easily because there are as many $\delta-$functions as there as momentum integration variables. We begin by introducing auxiliary momentum fields Π_i $(i = 1 \ldots N_\Pi)$, which correspond to the momentum fields at each kernel eigenvalue crossing during the trajectory. The gauge field at the crossing is U_i, leading to a reflection condition depending on a variable x_i. These additional momentum fields are, of course, precisely determined from either the initial momenta using the trajectory $T_i[\Pi, \Phi, U,]$, or from the final momenta and the reverse trajectory $T_i^{-1}[\Pi', \Phi, U']$; and these conditions lead to a delta-function in the integral for each auxiliary momentum field introduced. Since the various x_is are not degenerate with respect to the initial gauge field and momentum, we can write $\prod(1 + \delta(x_i)) = 1 + \sum \delta(x_i)$. Using this notation, the detailed balance equation reads

$$
\int d\Phi^\dagger d\Phi P[U' \leftarrow U, \Phi] W_c[U, \Phi] = \int d\Pi' d\Pi d\Phi^\dagger d\Phi \prod d\Pi_i P_A
$$
$$
\left(\delta([\Pi', \Phi, U'] - T_{MD}[\Pi, \Phi, U]) \prod_{j=1}^{N_\Pi} \delta([\Pi_j, \Phi, U_j] - T_i[\Pi, \Phi, U]) + \right.
$$
$$
\left. \sum_{i=1}^{N_\pi} \delta(x_i) J(x_i) \prod_{j=1}^{i} \delta([\Pi_i, \Phi, U_i] - T_i[\Pi, \Phi, U]) \prod_{j=i+1}^{N_\Pi} \delta([\Pi_i, \Phi, U_i] - T_i^{-1}[\Pi', \Phi, U']) \right).
$$
$$
\text{(A.52)}
$$

$J(x_i)$ is the coefficient of the $\delta-$function in the Jacobian. Using the notation of equation (46), we can convert the delta function from a function of x to

a function of (Π_i, η_k) by multiplying by $\frac{1}{dx/d(\Pi_i, \eta_k)}$, and summing over each possible solution for (Π_i, η_k) which gives $x = 0$. Since x is quadratic in each (Π_i, η_k), which corresponds to one component of the momentum field, there will be two possible solutions to the equation $x = 0$ for each of the N_k momentum field components; and we will generate a $\delta-$function for each of these solutions. Using $x = 1 + 4d/(\sum_k (\eta_k, \Pi_i)^2$, it follows that

$$\delta(x_i)J(x_i) = 2\sum_k \left[\delta\left((\Pi_i, \eta_k) - \sqrt{-\left(4d + \sum_{m \neq k} (\Pi_i, \eta_m)^2 \right)} \right) \frac{(\Pi_i, \eta_k)\eta_k}{\sum_n (\Pi_i, \eta_n)^2} + \right.$$
$$\left. \delta\left((\Pi_i, \eta_k) + \sqrt{-\left(4d + \sum_{m \neq k} (\Pi_i, \eta_m)^2 \right)} \right) \frac{(\Pi_i, \eta_k)\eta_k}{\sum_n (\Pi_i, \eta_n)^2} \right] J(x_i).$$
(A.53)

It is easily observed that the coefficient of the $\delta-$function for each k is an odd function of (Π_i, η_k) multiplied by $J(x_i)$. In particular, if $J(x_i)$ is an even function of (Π_i, η_n), then the coefficients for the positive (Π_i, η) and negative (Π_i, η) δ-functions will precisely cancel, removing all the $\delta-$function terms from the detailed balance equation. So the task of demonstrating that this $\delta-$function will not contribute to the final ensemble can be reduced to a demonstration that $J(x)$ is an even function of the momenta.

From equation (A.42), we see that $J(x) = \partial x/\partial(\Pi, \eta_j)(F_{Ti}^{\Pi} - F_{Ri}^{\Pi})$. The Jacobian is the determinant of the $N_k \times N_k$ square matrix

$$(\eta_i, F_T^{\Pi} - F_{Ri}^{\Pi})\partial x/\partial(\Pi, \eta_j)\delta(x) + \ldots.$$
(A.54)

Noting that $(\eta_i, F_T^{\Pi}) = 0$ at $x = 0$, this matrix is the outer product of two vectors, both of which are odd functions of (η_j, Π_i). Therefore, $J(x_i)$ is an even function of (η_j, Π_i). As previously argued, this means that the presence of the $\delta-$function will not affect the final ensemble. We demonstrate that $J(x_i)$ is even for an explicit example below.

It might be thought that this argument might be invalid because we cannot sample both positive and negative Π with equal probability. If the trajectory starts in one particular topological sector, then it can only approach the topological wall from one direction (unless there is more than topological index change in the trajectory). However, our calculation does not depend on the sign of Π but the sign of (Π, η). The algorithms presented in this article are all even functions of η; in practice, the sign of η will be chosen randomly. In the detailed balance equation, since the both the molecular dynamics trajectory, T, and the metropolis acceptance probability, P_A, are independent of the sign of η, both choices for η lead to the same final gauge field, and we must include this choice of sign by summing over the two possibilities, weighting them by the appropriate probability; if the algorithm is designed without bias,

this probability will be $1/2$. In other words, it is not the integration over the auxiliary momentum fields but this sum over the signs of η which causes the $\delta-$functions to cancel. Thus the direction in which the trajectory approaches the topological sector wall, and the limited sampling of the momentum fields are both unimportant.

As an example, we now explicitly calculate the Jacobian for one particular case to demonstrate how this works in practice. We assume that there is just one momentum crossing in the trajectory, and use the update

$$
\begin{aligned}
F_{Ti}^{\Pi} =& \pi_i^- + \eta_i(\Pi^-, \eta) \left(\sqrt{1 + \frac{4d}{(\Pi^-, \eta)^2}} - 1 \right) - \\
& \tau_c((F_i^- + F^+) - \eta_i(\eta, F^- + F^+)) \\
F_{Ri}^{\Pi} =& \pi_i^- - 2\eta_i(\eta, \Pi^-) - 2\tau_c(F_i^- - \eta_i(\eta, F^-)) \\
F_{Ti}^{U} =& q_i^- + \tau_c(F_{Ti}^{\Pi} - \pi_i^-) \\
F_{Ri}^{U} =& q_i^- + \tau_c(F_{Ri}^{\Pi} + \pi_i^-) \\
x =& 1 + \frac{4d}{(\Pi^-, \eta)^2} \\
\left(\frac{\partial x}{\partial(\Pi^-, \eta)} \right) \Bigg|_{x=0} =& - \frac{2\eta}{(\Pi^-, \eta)} \\
(F_{Ti}^{\Pi} - F_{Ri}^{\Pi}) \Big|_{x=0} =& (\Pi^-, \eta) \\
J(x) = \left(\frac{\partial x}{\partial(\Pi^-, \eta)} \right) \Bigg|_{x=0} & (F_{Ti}^{\Pi} - F_{Ri}^{\Pi}) \Big|_{x=0} = -2. \qquad (A.55)
\end{aligned}
$$

Hence J is an even function of (Π, η). The additional and unwanted term in the detailed balance equation, once we have integrated out all the auxiliary momentum integration variables except (Π_i, η), reads

$$
-2 \int d\Phi^\dagger d\Phi \sum_{\pm\eta} \int (\Pi_i, \eta) \left[\delta((\Pi_i, \eta_i) - \sqrt{-4d}) \frac{1}{(\Pi_i, \eta_i)} + \delta((\Pi_i, \eta_i) + \right.
$$
$$
\left. \sqrt{-4d}) \frac{1}{(\Pi_i, \eta_i)} \right] P_A = 0
$$
$$
(A.56)
$$

Hence the detailed balance condition is, in fact, maintained despite the δ-functions in the Jacobian.

Numerically, in section 5.4, we have compared the algorithm with an approach that explicitly does satisfy detailed balance (reflecting when $|d| > d_{max}$ and using $\Pi^+ = \Pi^-$ when $|d| < d_{max}$), but does not necessarily conserve energy. In an extensive simulation we found no difference in the observables calculated.

A.3 Correction step error of $O(\tau^2)$

Suppose that there is a crossing between time $\tau = 0$ (where the gauge field, momentum, and fermionic force are U_0, Π_0 respectively), and time $\tau = \Delta\tau$ (with gauge field U_1, momentum Π_1). The gauge fields immediately before and after the eigenvalue crossing are U_d and U_u.[17] If $S(U) = E - \frac{1}{2}\Pi^2$ is the action, then the total force F' acting on the momentum is

$$f_i^{x\mu}(U) = \frac{\partial S(U)}{\partial r_i^{x\mu}} = -\frac{\partial \pi_i^{x\mu}}{\partial \tau}.$$
(A.57)

We shall demonstrate that the energy difference, ΔE, between time $\tau = \Delta\tau$ and time $\tau = 0$ is of order $\Delta\tau^2$. The energy change between time $\Delta\tau$ and time 0 is

$$\Delta E = \frac{1}{2}(\Pi_1, \Pi_1) - \frac{1}{2}(\Pi_0, \Pi_0) + S(U_1) - S(U_0).$$
(A.58)

In this notation, our update for transmission (50), with $s_1^2 = 1$), and neglecting terms of $O(\Delta\tau^2)$ or higher is

$$\Pi^- = \Pi_0 - \frac{\Delta\tau}{2}F_0;$$

$$\Pi^+ = \Pi^- - \tau_c\left(1 - |\eta\rangle\langle\eta|\right)\left(F^- - F^+\right) + \tau_c\frac{1}{3}\mathrm{Tr}(F^- - F^+)+$$

$$\eta(\eta, \Pi^-)\sqrt{1 + \frac{4d}{(\eta, \Pi^-)^2}}+$$

$$\left(\eta_1^2(\eta_1^2, \Pi^- - \frac{\tau_c}{2}(F^- + F^+)) + \eta_2^2(\eta_2^2, \Pi^- - \frac{\tau_c}{2}(F^- + F^+))\right) \times$$

$$\left(\sqrt{1 - 2\frac{\tau_c(F^-, \eta)(\Pi^-, \eta) - \tau_c(F^+, \eta)(\Pi^+, \eta)}{(\eta_1^2, \Pi^- - \frac{\tau_c}{2}(F^- + F^+))^2 + (\eta_2^2, \Pi^- - \frac{\tau_c}{2}(F^- + F^+))^2}} - 1\right);$$

$$\Pi_1 = \Pi^+ - \frac{\Delta\tau}{2}F_1$$

$$U^- = e^{i\frac{\Delta\tau}{2}\Pi^-}U_0$$

$$U^+ = e^{-i\tau_c\Pi^+}e^{+i\tau_c\Pi^-}U^-$$

$$U_1 = e^{i\frac{\Delta\tau}{2}\Pi^+}U^+$$
(A.59)

$$U_d = e^{i\left(\frac{\Delta\tau}{2}+\tau_c\right)\Pi^-}U_0$$

$$U_1 = e^{i\left(\frac{\Delta\tau}{2}-\tau_c\right)\Pi^+}U_u.$$
(A.60)

---

[17] Note that in practice $U_u = U_d = U_c$ - there is no discontinuity in the gauge field at the crossing. The notation here is purely for clarification.

There is a jump in the action S at the eigenvalue crossing,

$$S(U_u) - S(U_d) = -2d. \tag{A.61}$$

Using $(\Pi_+ - \Pi_-, F_+ - F_-) = O(\Delta\tau^2)$, we can show that

$$
\begin{aligned}
(\Pi^+, \Pi^+) - (\Pi^-, \Pi^-) =& 4d + 2\tau_c(\Pi^-, F^+) - 2\tau_c(\Pi^-, F^-) + \\
& \tau_c(\Pi_+ - \Pi_-, F_+ + F_-) + O(\Delta\tau^2) \\
=& 4d + 2\tau_c(\Pi^-, F^+) - 2\tau_c(\Pi^-, F^-) + O(\Delta\tau^2), \quad (A.62)
\end{aligned}
$$

$$
\begin{aligned}
(\Pi_1, \Pi_1) - (\Pi_0, \Pi_0) =& 4d - \Delta\tau((\Pi_0, F_0) + (\Pi_1, F_1)) \\
& - 2\tau_c((F_0, \Pi^-) - (F_1, \Pi^+)) + O(\Delta\tau^2), \quad (A.63)
\end{aligned}
$$

$$
\begin{aligned}
S(U_1) - S(U_0) =& S\left(U\left(r_{ci}^+ + \left(\frac{\Delta\tau}{2} - \tau_c\right)p_i\right)\right) \\
& - S\left(U\left(r_{ci}^- + \left(\frac{\Delta\tau}{2} + \tau_c\right)\pi_i\right)\right) + O(\Delta\tau^2) \\
=& S(U_u) - S(U_d) + \left(\frac{\Delta\tau}{2} - \tau_c\right)\frac{\partial S}{\partial r_i}\bigg|_{r_c^+} p_i + \\
& \left(\frac{\Delta\tau}{2} + \tau_c\right)\frac{\partial S}{\partial r_i}\bigg|_{r_c^-} \pi_i + O(\Delta\tau^2) \\
=& -2d + \frac{\Delta\tau}{2}\left((\Pi^+, F_1) + (\Pi^-, F_0)\right) + \\
& \tau_c((\Pi^-, F^-) - (\Pi^+, F^+)) + O(\Delta\tau^2). \quad (A.64)
\end{aligned}
$$

So,

$$\Delta E = O(\Delta\tau^2). \tag{A.65}$$

Therefore, our modified correction update for transmission conserves energy up to $O(\Delta\tau^2)$. It can also be shown that the energy violating reflection term is also $O(\Delta\tau^2)$. Without the additional correction term to account for the $O(\Delta\tau)$ error, the energy violation would be

$$\frac{\tau_c}{2}\left(\left(F^- - F^+, \eta\right)(\Pi^- + \Pi^+, \eta) - \left(F^- + F^+, \eta\right)(\Pi^- - \Pi^+, \eta)\right) + O(\Delta\tau). \tag{A.66}$$

B Two Crossings within the same Molecular Dynamics Step

There are several situations when it is difficult to resolve whether or not there has been an eigenvalue crossing. Firstly, when an eigenvalue has a minimum

close to zero, and secondly when there are two small eigenvalues. In the first case, one can identify the minimum by looking at the sign of the differential of the eigenvalue with respect to computer time. If the eigenvalue is sufficiently small that there is a danger that the crossing may have occurred, one can search for the zero eigenvalue. In the second case one has to search for crossings if there is a large mixing between the two eigenvectors, or an initial Newton-Raphson extrapolation indicates that they might cross. In both cases, one moves to the point of the first crossing, changes the momentum in the usual manner, moves to the second crossing (if necessary, i.e. the first crossing was transmission), and changes the momentum again. Care needs to be taken to ensure that the algorithm will detect the potential crossing in both directions, otherwise there could be a breakdown in reversibility.

More serious is the possibility of mixing between a small positive and small negative eigenvalues of the kernel operator. As an example, let us consider a system with just two eigenvectors $|\psi_1\rangle$ and $|\psi_2\rangle$. One can calculate the mixing between the eigenvectors using a similar method to the one used in section 2.2, except in this case we will not expand in small $\Delta\tau$. One starts as before with the eigenvalue equations at times τ and $\tau + \Delta\tau$:

$$
\begin{aligned}
Q|\psi_1\rangle &= \lambda_1|\psi_1\rangle \\
Q|\psi_2\rangle &= \lambda_2|\psi_2\rangle \\
|\psi_1\rangle + |\delta_1\rangle &= \cos\theta|\psi_1\rangle + e^{i\phi}\sin\theta|\psi_2\rangle \\
|\psi_2\rangle + |\delta_2\rangle &= \cos\theta|\psi_2\rangle + e^{-i\phi}\sin\theta|\psi_1\rangle.
\end{aligned}
\tag{B.1}
$$

One can now easily solve for the mixing angles θ and ϕ:

$$
\begin{aligned}
e^{i\phi} &= \sqrt{\frac{\langle\psi_2|\delta Q|\psi_1\rangle}{\langle\psi_2|\delta Q|\psi_1\rangle}} \\
A &= \frac{(\lambda_2 - \lambda_1 + \langle\psi_2|\delta Q|\psi_2\rangle - \langle\psi_1|\delta Q|\psi_1\rangle)^2}{4\langle\psi_2|\delta Q|\psi_1\rangle\langle\psi_1|\delta Q|\psi_2\rangle} \\
\tan^2\theta &= A\left(\sqrt{1 + \frac{1}{A}} - 1\right)^2.
\end{aligned}
\tag{B.2}
$$

An expansion in small $\delta\tau$ (with $\delta Q = \delta\tau\partial Q/\partial\tau + O(\delta\tau^2)$) gives the same expression that was derived in section 2.2. However, this expansion is only valid if

$$
\left|\frac{\langle\psi_2|\delta Q|\psi_2\rangle - \langle\psi_1|\delta Q|\psi_1\rangle}{\lambda_2 - \lambda_1}\right| \ll 1
$$

and

$$
\left|\frac{\langle\psi_1|\delta Q|\psi_2\rangle\langle\psi_2|\delta Q|\psi_1\rangle}{(\lambda_2 - \lambda_1)^2}\right| \ll 1.
$$

These conditions fail if two eigenvalues are close to each other and both have maxima or minima in the same time step. One can write the fermionic force contribution from the small eigenvectors (excluding the delta function term) as

$$2 \lim_{\delta\tau \to 0} \frac{1}{\delta\tau} \sin\theta \cos\phi \langle X| \left\{ \gamma_5, |\psi_1\rangle\langle\psi_2| + |\psi_2\rangle\langle\psi_1| \right\} |X\rangle (\epsilon(\lambda_1) - \epsilon(\lambda_2)).$$

If there occurs a small negative eigenvalue and a small positive eigenvalue—mixing between eigenvectors with the same sign does not contribute to the force—and they have minima at the same time step, there could potentially emerge a very large fermionic force.

In our simulations we have indeed observed this effect. Most of the metropolis rejections on larger lattices can be traced back to it. In a subsequent paper we are going to describe a solution to this problem [55].

References

[1] Michael Creutz, The saga of rooted staggered quarks 0804.4307.

[2] D. B. Kaplan, A Method for simulating chiral fermions on the lattice, Phys. Lett. B288 (1992) 342–347, hep-lat/9206013.

[3] H. B. Nielsen and B. Ninomiya, Nucl. Phys B185 (1981) 20.

[4] R. Narayanan and H. Neuberger, Chiral fermions on the lattice, Phys. Rev. Lett. 71 (1993) 3251–3254, hep-lat/9308011.

[5] H. Neuberger, Exactly massless quarks on the lattice, Phys. Lett. B417 (1998) 141–144, hep-lat/9707022.

[6] P. Hasenfratz, Prospects for perfect actions., Nucl.Phys.Proc.Suppl. 63 (1998) 53–58, hep-lat/9709110.

[7] P. H. Ginsparg and K. G. Wilson, A remnant of chiral symetry on the lattice, Phys. Rev. D25 (1982) 2649.

[8] M. Lüscher, Abelian chiral gauge theories on the lattice with exact gauge invariance, Nucl. Phys. B549 (1999) 295–334, hep-lat/9811032.

[9] P. Hernández, K. Jansen, and L. Lellouch, Finite-size scaling of the quark condensate in quenched lattice QCD, Phys. Lett. B469 (1999) 198–204, hep-lat/9907022.

[10] P. Hernández, K. Jansen, and L. Lellouch, Chiral symmetry breaking from Ginsparg-Wilson fermions, Nucl. Phys. Proc. Suppl. 83 (2000) 633–635, hep-lat/9909026.

[11] P. Hernández, K. Jansen, and L. Lellouch, A Numerical treatment of Neuberger's Lattice Dirac Operator, in: Frommer et al. [82], pp. 29–39, proceedings of the International Workshop, University of Wuppertal, August 22-24, 1999.

[12] B. Bunk, hep-lat/9805030 (1998).

[13] P. Hernández, K. Jansen, and M. Lüscher, A note on the practical feasibility of domain-wall fermions, hep-lat/0007015 (2000).

[14] A. Boriçi, Fast methods for computing the Neuberger operator, in: Frommer et al. [82], pp. 40–47, proceedings of the International Workshop, University of Wuppertal, August 22-24, 1999.

[15] A. Boriçi, A Lanczos approach to the inverse square root of a large and sparse matrix, J. Comput. Phys. 162 (2000) 123, hep-lat/9910045.

[16] A. Boriçi, On the Neuberger overlap operator, Phys. Lett. B453 (1999) 46–53, hep-lat/9810064.

[17] H. A. van der Vorst, Solution of $f(A)x = b$ with Projection Methods, in: Frommer et al. [82], pp. 18–28, proceedings of the International Workshop, University of Wuppertal, August 22-24, 1999.

[18] H. Neuberger, A practical implementation of the overlap-Dirac operator, Phys. Rev. Lett. 81 (1998) 4060–4062, hep-lat/9806025.

[19] H. Neuberger, Overlap Dirac Operator, in: Frommer et al. [82], proceedings of the International Workshop, University of Wuppertal, August 22-24, 1999.

[20] R. G. Edwards, U. M. Heller, J. Kiskis, and R. Narayanan, Chiral condensate in the deconfined phase of quenched gauge theories, Phys. Rev. D61 (2000) 074504, hep-lat/9910041.

[21] R. G. Edwards, U. M. Heller, and R. Narayanan, A study of practical implementations of the overlap-Dirac operator in four dimensions, Nucl. Phys. B540 (1999) 457–471, hep-lat/9807017.

[22] J. van den Eshof, A. Frommer, Th. Lippert, K. Schilling, and H.A. van de Vorst, Numerical Methods for the QCD overlap Operator: I. Sign-Function and Error Bounds, Comput. Phys. Comm. 146 (2002) 203–224.

[23] R. V. Gavai, S. Gupta, and R. Lacaze, Speed and adaptability of overlap fermion algorithms, Comput. Phys. Commun. 154 (2003) 143–158, hep-lat/0207005.

[24] S. J. Dong et al., Chiral logs in quenched QCD, hep-lat/0304005.

[25] T. Chiu, T. Hsieh, C. Huang, and T. Huang, A note on the Zolotarev optimal rational approximation for the overlap Dirac operator, phys. Rev. D66 (2002) 114502, hep-lat/0206007.

[26] Z. Fodor, S. D. Katz, and K. K. Szabo, Dynamical overlap fermions, results with hybrid Monte-Carlo algorithm, JHEP 08 (2004) 003, hep-lat/0311010.

[27] T. Chiu, Optimal domain-wall fermions, Phys. Rev. Lett. 90 (2003) 071601, hep-lat/0209153.

[28] T. Chiu, Locality of optimal lattice domain-wall fermions, Phys. Lett. B552 (2003) 97–100, hep-lat/0211032.

[29] T. Chiu, Optimal lattice domain-wall fermions with finite N(s), hep-lat/0304002 (2003).

[30] A. Borici, A. D. Kennedy, B. J. Pendleton, and U. Wenger, The overlap operator as a continued fraction, Nucl. Phys. Proc. Suppl. 106 (2002) 757–759, hep-lat/0110070.

[31] H. Neuberger, The overlap lattice Dirac operator and dynamical fermions, Phys. Rev. D60 (1999) 065006, hep-lat/9901003.

[32] U. Wenger, The overlap Dirac operator as a continued fraction. Hep-lat/0403003.

[33] C. Liu, Hybrid Monte Carlo algorithm for lattice QCD with two flavors of dynamical Ginsparg-Wilson quarks, Nucl. Phys. B554 (1999) 313–322, hep-lat/9811008.

[34] P. Hernández, K. Jansen, and L. Lellouch, A numerical treatment of Neuberger's lattice Dirac operator, in: A. Frommer (Ed.), Wuppertal 1999, Numerical challenges in lattice quantum chromodynamics, 2000, pp. 29–39, hep-lat/0001008.

[35] K. Jansen, Overlap and domain wall fermions: What is the price of chirality?, Nucl. Phys. Proc. Suppl. 106 (2002) 191–192, hep-lat/0111062.

[36] L. Giusti, C. Hoelbling, and C. Rebbi, Light quark masses with overlap fermions in quenched QCD, Phys. Rev. D64 (2001) 114508, hep-lat/0108007.

[37] L. Giusti, C. Hoelbling, M. Lüscher, and H. Wittig, Numerical techniques for lattice QCD in the epsilon-regime, Comput. Phys. Commun. 153 (2003) 31–51, hep-lat/0212012.

[38] S. Duane, A. Kennedy, B. Pendelton, and D. Roweth, Phys. Lett. B195 (1987) 216.

[39] A. Bode, U. M. Heller, R. G. Edwards, and R. Narayanan, First experiences with HMC for dynamical overlap fermions, in: Dubna 1999, Lattice fermions and structure of the vacuum, 1999, pp. 65–68, hep-lat/9912043.

[40] S. Dürr and Ch. Hoelbling, Staggered versus overlap fermions: A study in the Schwinger model with N(f) = 0,1,2, Phys. Rev. D69 (2004) 034503, hep-lat/0311002.

[41] L. Giusti, Ch. Hoelbling, and C. Rebbi, Schwinger model with the overlap-Dirac operator: Exact results versus a physics motivated approximation, Phys. Rev. D64 (2001) 054501, hep-lat/0101015.

[42] S. Dürr and C. Hoelbling, Scaling tests with dynamical overlap and rooted staggered fermions Hep-lat/0411022.

[43] Z. Fodor, S. D. Katz, and K. K. Szabo, Dynamical overlap fermions, results with HMC algorithm, Nucl. Phys. Proc. Supp. 140C, hep-lat/0409070.

[44] T. DeGrand and S. Schaefer, Physics issues in simulations with dynamical overlap fermions Hep-lat/0412005.

[45] P. Hernandez, K. Jansen, and M. Lüscher, Locality properties of Neuberger's lattice Dirac operator, Nucl. Phys. B552 (1999) 363–378, hep-lat/9808010.

[46] G. Arnold, N. Cundy, J. van den Eshof, A. Frommer, S. Krieg, Th. Lippert, and K. Schäfer, Numerical methods for the QCD overlap operator. II: Optimal Krylov subspace methods To appear in the proceedings of the Third International Workshop on Numerical Analysis and Lattice QCD, hep-lat/0311025.

[47] N. Cundy, J. van den Eshof, A. Frommer, S. Krieg, Th. Lippert, and K. Schäfer, Numerical methods for the QCD overlap operator. III: Nested iterations., Comp. Phys. Comm. 165 (2005) 841, hep-lat/0405003.

[48] S. Krieg et al., Improving inversions of the overlap operator, Nucl. Phys. Proc. Supp. 140C, hep-lat/0409030.

[49] N. Cundy, S. Krieg, A. Frommer, Th. Lippert, and K. Schilling, Dynamical overlap simulations using HMC, Nucl. Phys. Proc. Supp. 140C (2005) 841, hep-lat/0409029.

[50] I. P. Omelyan, I. M. Mrygloda, and R. Folk, Symplectic analytically integrable decomposition algorithms: classification, derivation, and application to molecular dynamics, quantum and celestial mechanics simulations, Computer Physics Communications 151 (2003) 272.

[51] Tetsuya Takaishi and Philippe de Forcrand, Testing and tuning new symplectic integrators for hybrid Monte Carlo algorithm in lattice QCD, Phys. Rev. E73 (2006) 036706, hep-lat/0505020.

[52] J. C. Sexton and D. H. Weingarten, Nucl. Phys. B 380 (1992) 665.

[53] D. Ingerman, V. Druskin, and L. Knizerhman, Comm. Pure Appl. Math. 53 (2000) 1039.

[54] P. P. Petrushev and V. A. Popov, Rational approximation of real functions, Cambridge University Press, 1987.

[55] Nigel Cundy, Small Wilson Dirac operator eigenvector mixing in dynamical overlap hybrid Monte-Carlo 0706.1971.

[56] Nigel Cundy, Stefan Krieg, Thomas Lippert, and Andreas Schäfer, Dynamical overlap fermions with increased topological tunnelling, PoS LATTICE (2007) 030, 0710.1785.

[57] Thomas DeGrand and Stefan Schaefer, Chiral properties of two-flavor QCD in small volume and at large lattice spacing, Phys. Rev. D72 (2005) 054503, hep-lat/0506021.

[58] H. Neff, Efficient computation of low-lying eigenmodes of non-Hermitian Wilson-Dirac type matrices, Nucl. Phys. Proc. Suppl. 106 (2002) 1055–1057, hep-lat/0110076.

[59] http://www.caam.rice.edu/software/ARPACK/.

[60] T. Kalkreuter and H. Simma, An Accelerated conjugate gradient algorithm to compute low lying eigenvalues: A Study for the Dirac operator in SU(2) lattice QCD, Comput. Phys. Commun. 93 (1996) 33–47, hep-lat/9507023.

[61] Nigel Cundy, Current status of dynamical overlap project, Nucl. Phys. Proc. Suppl. 153 (2006) 54–61, hep-lat/0511047.

[62] Thomas Degrand and Stefan Schaefer, Simulating an arbitrary number of flavors of dynamical overlap fermions, JHEP 07 (2006) 020, hep-lat/0604015.

[63] Nigel Cundy, Stefan Krieg, Thomas Lippert, and Andreas Schäfer, Topological tunneling with Dynamical overlap fermions ArXiv:0803.0294[hep-lat].

[64] Nigel Cundy, Stefan Krieg, Thomas Lippert, and Andreas Schäfer, forthcoming.

[65] G. I. Egri, Z. Fodor, S. D. Katz, and K. K. Szabo, Topology with Dynamical Overlap Fermions Hep-lat/0510117.

[66] Hidenori Fukaya, Shoji Hashimoto, Takuya Hirohashi, Kenji Ogawa, and Tetsuya Onogi, Topology conserving gauge action and the overlap-Dirac operator, Phys. Rev. D73 (2006) 014503, hep-lat/0510116.

[67] R. P. Brent, Algorithms for minimization without Derivitives, Englewood Cliffs, NJ, 1973.

[68] W. Press, S. Teukolsky, W. Vetterling, and B. Flannery, Numerical Recipies in Fortran, 2nd Ed., Cambridge University Press, 1992.

[69] N. Garron, L. Giusti, Ch. Hoelbling, L. Lellouch, and C. Rebbi, B(K) from quenched QCD with exact chiral symmetry, Phys. Rev. Lett. 92 (2004) 042001, hep-ph/0306295.

[70] R. G. Edwards, U. M. Heller, and R. Narayanan, The overlap-Dirac operator: Topology and chiral symmetry breaking, Chin. J. Phys. 38 (2000) 594–604, hep-lat/0001013.

[71] R. G. Edwards, U. M. Heller, and R. Narayanan, A study of practical implementations of the overlap-Dirac operator in four dimensions, Nucl. Phys. B540 (1999) 457–471, hep-lat/9807017.

[72] Z. Fodor, private communication.

[73] R. J. Crewther, Phys.Lett. B70 (1977) 349.

[74] P. Di Vecchia and G. Veneziano, Nucl Phys B171 (1980) 253.

[75] H. Leutwyler and A. Smilga, Phys. Rev. D45 (1992) 5607.

[76] C. Bernard et al., Topological susceptibility with the improved Asqtad action, Phys. Rev. D68 (2003) 114501, hep-lat/0308019.

[77] G. S. Bali et al., Quark mass effects on the topological susceptibility in QCD, Phys. Rev. D64 (2001) 054502, hep-lat/0102002.

[78] S. Dürr, Topological susceptibility in full QCD: Lattice results versus the prediction from the QCD partition function with granularity, Nucl. Phys. B611 (2001) 281–310, hep-lat/0103011.

[79] Stefan Schaefer, Algorithms for dynamical overlap fermions, PoS LAT2006 (2006) 020, hep-lat/0609063.

[80] N. Cundy, Zero mode topology with dynamical overlap fermions, in: XXIVth International Symposium on Lattice Field Theory, 2006.

[81] I. Montvay and G. Münster, Quantum Fields on a Lattice, Cambridge University Press, 1994.

[82] A. Frommer, Th. Lippert, B. Medeke, and K. Schilling (Eds.), Numerical Challenges in Lattice Quantum Chromodynamics, Lecture Notes in Computational Science and Engineering, Springer Verlag, Heidelberg, 2000, proceedings of the International Workshop, University of Wuppertal, August 22-24, 1999.